Microporous and Mesoporous Materials 254 (2017) 96–113

Contents lists available at ScienceDirect

Microporous and Mesoporous Materials

journal homepage: www.elsevier.com/locate/micromeso

Vanadium oxide supported on mesoporous SBA-15 modified with Al and Ga as a highly active catalyst in the ODS of DBT

Lorena Rivoira, María L. Martínez, Oscar Anunziata, Andrea Beltramone*

Centro de Investigación en Nanociencia y Nanotecnología (NANOTEC), Facultad Regional Córdoba, Universidad Tecnológica Nacional, Maestro López y Cruz Roja Argentina, 5016, Córdoba, Argentina

ARTICLE INFO

Article history:
Received 28 September 2016
Received in revised form
10 April 2017
Accepted 11 April 2017
Available online 12 April 2017

Keywords:
VOx supported SBA-15
Dibenzothiophene
Ultra-low-sulfur diesel
Deactivation
Gallium
Aluminum

ABSTRACT

Vanadium oxides supported on mesoporous SBA-15 catalysts with different vanadium loadings were studied in the oxidative desulfurization (ODS) of dibenzothiophene as a model sulfur compound. The catalytic activity was improved when SBA-15 framework was modified by adding Al and Ga. Structural and textural characterization of the catalysts were performed by means of XRD, N_2 adsorption, UV–Vis–DRS, XPS, NMR, TEM, Raman, TPR and Py-FTIR. UV–Vis–DRS and Raman demonstrated that highly dispersed vanadium VO_4^{-3} species are responsible for the high activity in the sulfur removal. The Ga modified support with an intermediate V/Si ratio of 1/30 was the most active catalyst for ODS of DBT, using hydrogen peroxide as oxidant and acetonitrile as solvent. 100% of DBT elimination was attained at a short time in mild conditions. Gallium and aluminum incorporation into the support modified successfully the nature of the SBA-15 surface by generating Bronsted and Lewis acidity. The interaction between the acid sites with the active vanadium sites improved the activity of the catalysts. The high dispersion depended on the vanadium loading and on the nature of the support. The more acidic support allowed better dispersion of the vanadium species due to stronger interaction metal-support. The reusability of the catalysts indicates that vanadium oxide supported on mesoporous SBA-15 modified with Ga and Al are potential catalysts for the ODS of dibenzothiophene.

1. Introduction

Ultra-low-sulfur diesel (ULSD) is diesel fuel with substantially lowered sulfur content. Although there is no single standard set of specifications, refineries all over the world are applying them to reduce sulfur levels in transportation fuels in order to satisfy the upcoming regulation established in each country. In order to adapt current processes to these strict regulatory requirements, several technologies have been developed for deep desulfurization of diesel fuel. The major portion of sulfur in light cycle oils (LCO) is found in dibenzothiophene (DBT) and alkyl-dibenzothiophenes, which are not easily removable by hydrotreating, because they require high pressure and hydrogen consumption [1].

However, there is an alternative method for deep sulfur elimination from light oils, the oxidative desulfurization (ODS). This process was reported in literature as early as 1954 and it was not considered as a potential process until the imposed current regulations requiring the production of ultra-low sulfur diesel. ODS has been extensively studied probably due to its attractive properties, including lower temperature and pressure conditions and lower operating costs compared with those found in conventional hydrodesulfurization processes. Oxidation of organosulfur compounds results in the formation of sulfoxides/sulfones, highly polar and hence easily removed either by extraction into polar solvents or by adsorption. The oxidation of DBTs with organic hydroperoxides or H_2O_2 was studied over various catalytic heterogeneous systems, such as oxide-supported metals or titanium silicalites [2–16]. The oxidation of DBTs was also performed using WO_x/ZrO_2 catalyst [17], supported Pd, Cr_2O_3, unsupported manganese oxides and a commercial $Co–Mo/Al_2O_3$ with hydrogen peroxide as oxidant [18]. Vanadosilicates as catalysts for desulfurization of light oil

* Corresponding author.
E-mail address: abeltramone@frc.utn.edu.ar (A. Beltramone).

http://dx.doi.org/10.1016/j.micromeso.2017.04.019
1387-1811/

under mild reaction conditions were used by Cedeño-Caero et al. [19]. They achieved removal of sulfur compounds present in diesel with a yield higher than 80% using hydrogen peroxide as oxidizing agent and acetonitrile as solvent. Yasuhiro Shiraishi et al. [20] compared the catalytic activity of three types of vanadosilicates, having different pore-size distribution with those of the corresponding titanosilicates. They found that mesoporous vanadosilicates showed the highest activity [21]. Likewise, Y. Liu et al. [22] used metal oxides as supports and they proved that the catalytic behavior of supported vanadium oxide catalysts in the selective oxidation reactions largely depended on the content of vanadium loaded on the support.

The use of large-surface-area materials with ordered porous structure, such as mesoporous molecular sieves, is an interesting alternative for catalytic ODS reaction. The intrinsic characteristics of these materials make them particularly promising for application in oil refining. SBA-16 and CMK-3 have been already tested in our recent studies as supports of vanadium and titanium oxides, from which we have obtained very good results in removing sulfur [23,24]. Guoan Du et al. [25] synthesized vanadium oxide grafted on mesoporous silica SBA-15 using a controlled grafting process. They found that for V-SBA-15 samples with higher vanadium loading, the reactive conversion approached 100%, and the temperature for the maximum conversion decreased with increasing vanadium loading. Cedeño-Caero et al. [16] tested the ODS of DBT using vanadium oxides supported over SBA-15 and compared their activity with other supports. They found that the activity largely depended on the characteristics of the support and its interaction with the active species.

According to previous studies, when tetravalent cations like Ti^{4+}, Zr^{4+}, V^{4+}, Sn^{4+}, etc. were incorporated into the framework of SBA-15, electroneutrality was maintained but some redox properties were incorporated into the support surface [23,26–29].

Recently, Ding et al. [30] prepared and applied an iron-based redox ionic liquid modified mesoporous SBA-15 as a novel catalyst to the removal of sulfur compounds in model diesel. Through extensive studies, they confirmed to have a catalyst system with high surface area, high accessibility for substrate and oxidant. They observed that the sulfur removal is much better using an extractive substance. A few years before, in 2013 Kye-Sung Cho et al. [31] found that the ODS for sulfur compounds proceed promptly with complete conversion applying Ti-SBA-15 catalyst. Therefore, based on literature SBA-15 is a desirable candidate for ODS due to wider pore size and considerably thicker pore walls, as well as thermal and hydrothermal stability. In order to improve the interaction between the mesoporous support and the vanadium active sites (VOx), we propose the modification of the silica framework via post-treatment with aluminum or gallium source. This modification in the nature of the support surface is expected to lead to efficiency improvement into ODS yields. It is well documented that aluminum incorporation into SBA-15 frameworks exhibits both Bronsted and Lewis acidities [32,33]. Ga-SBA-15 materials present weak acidity since gallium normally confers Lewis acidity, although it also induces the creation of Bronsted sites [34]. Acidity in the support can modify the interaction between the active species and the surface affecting dispersion and reducibility of the active species [32–34].

In this work we evaluate the activity of a series of catalysts, prepared using SBA-15 as support, in the ODS of dibenzothiophene as a model sulfur compound in a batch reactor under mild reaction conditions.

A series of vanadium supported on SBA-15, Al-SBA-15 and Ga-SBA-15 catalysts with different vanadium loadings were prepared. The objective of the work is to find the most efficient sulfur removal catalyst by combining a redox metal with a high area hydrothermal stable support.

2. Experimental

2.1. Synthesis of SBA-15

SBA-15 material has been synthesized according to the procedure described by Zhao et al. [35]. A solution of template was prepared by dissolving 1.5 g of P123 in 48 mL of HCl 2M (pH = 1). The solution was heating up to 50 °C, and then 3.7 mL (0.016 mol) of tetraethylorthosilicate (TEOS) were added dropwise under vigorous stirring. The mixture was held statically at constant temperature. After 24 h, temperature was set at 80 °C and maintained for 48 h. The solid obtained was then filtered and washed repeatedly with distilled water. Next, the material recovered was washed with a water/ethanol mixture for 2 h. Again, the material was filtered, washed and placed into an oven for drying at 100 °C. The material as synthesized was calcined at 500 °C for 5 h. Molar ratios of the synthesis were 1TEOS: 158 H_2O: 6HCl: 1.6×10^{-2} P123.

In order to incorporate the metal cations (Al, Ga) as isolated and very well dispersed species into the framework of SBA-15, we use the post-synthesis technique because the synthesis of SBA-15 materials involves strongly acidic conditions with pH below 1. Both aluminum and gallium sources in acidic solution remain in the cationic form and the introduction into the mesostructure walls is difficult. At low pH, the Al^{+3} and Ga^{+3} cations cannot polymerize or condense. Because of that, post-synthesis treatment is consequently an alternative method for the preparation of Al of Ga modified-SBA-15 materials.

2.2. Incorporation of Al and Ga via post-synthesis technique

In order to modify the acidic characteristics of the support, Al and Ga were incorporated in the matrix of SBA-15 using the following techniques: (i) post-synthesis alumination: pure silica SBA-15 (1 g) was stirred in 50 mL of aqueous solution containing sodium-aluminate ($NaAlO_2$), at room temperature for 20 h and pH of 5.6. The mixture was filtered, washed and dried at room temperature overnight and then calcined in air at 550 °C for 5 h. Since in the post-synthesis alumination method we used $NaAlO_2$ as source of Al, ion exchange procedure was performed in order to exchange sodium by NH_4^+. The ion exchange was carried out using 1M solution of NH_4Cl in contact with the aluminated sample for 40 h under stirring. After that, the sample was washed, filtered and dried, followed by calcination at 500 °C for 5 h, in order to obtain the protonated sample. The sample obtained with a theoretical ratio of Si/Al = 20 was denoted as Al-SBA-15. (ii) post-synthesis gallium incorporation: SBA-15 mesoporous material containing gallium was synthesized using an analogous procedure to alumination technique. An aqueous solution of $Ga(NO_3)_3$ was used as gallium source. The gallium concentration was calculated in order to obtain samples with Si/Ga ratio of 20. SBA-15 (1 g) material was mixed with 50 mL of the gallium solution at room temperature for 20 h. The sample was then filtered and washed with distilled water and dried at 60 °C overnight, to be finally calcined in air at 500 °C for 5 h. The material obtained was denoted as Ga-SBA-15.

2.3. Incorporation of V via direct-synthesis technique

The direct-synthesis technique and the post-synthesis technique were applied for the incorporation of vanadium cations in order to compare the efficiency of both methods in the dispersion, nature and reducibility of the vanadium species.

Firstly, vanadium was incorporated into the silica SBA-15 framework by direct-synthesis. Pluronic 123 surfactant was dissolved in a 2M HCl solution (pH < 3), then TEOS was added dropwise for about 10 min. VCl_3 was added to obtain a V/Si ratio of 1/30 and 1/54. The vanadium source was added under vigorous stirring for 5 additional min. Next, the synthesis followed as described previously for SBA-15. The materials obtained have been denominated as V-SBA-15 (y), where **y** refers to V/Si ratio.

2.4. Incorporation of V via post-synthesis technique

The wet impregnation method was used to incorporate vanadium species over SBA-15, Al-SBA-15 and Ga-SBA-15 supports via post-synthesis technique. To obtain samples with different vanadium loadings, 1 g of SBA-15 was added to several aqueous solutions with different contents of VCl_3. In order to dry off the product, the mixtures were placed into a rotary evaporator in vacuum at 70 °C and 70 rpm. Subsequently, the materials as synthetized were dried and finally calcined at 500 °C, with a heating rate of 3 °C/min. The samples were denoted as VOx-SBA-15 (y), where *x* depends on the oxidation state of vanadium and *y* is the V/Si ratio (1/54, 1/30, 1/18, 1/10 and 1/5). The incorporation of vanadium into Al-SBA-15 and Ga-SBA-15 with different V/Si ratios was performed using the same procedure as that described above. Samples were denoted as VOx-Al-SBA-15 (y) and VOx-Ga-SBA-15 (y).

2.5. Characterization of the catalysts

XRD patterns were collected by using a continuous scan mode. The scan speed was 0.02 deg (2 θ)/min in the Philips X'Pert PRO PANalytical diffractometer, operating with CuKα X-ray radiation (X-ray generator current and voltage set at 40 mA and 45 kV), using small divergence and scattering slits of 1/32 mm and a goniometer speed of 1.2° (2θ) min^{-1}. The scanning range was set between 0.5° and 5°. The sample was crushed previously and placed in an aluminum sample holder. Elemental analysis was performed by inductively coupled plasma-atomic emission spectroscopy (VISTA-MPX) operated with high frequency emission power of 1.5 kW and plasma airflow of 12.0 L/min. TPR was performed using a Micromeritics Chemisorb 2720 apparatus, with a flow of 14 mL/min of 10 mol% of H_2/N_2 heating up to 500 °C, with a preheating treatment at 380 °C in an inert atmosphere (N_2). N_2 adsorption/desorption isotherms at −196 °C were measured on ASAP 2020 equipment after degassing the samples at 400 °C. The pore size distribution of the samples was determined by the Nonlocal Density Functional Theory (NLDFT) applied for cylindrical pores of siliceous adsorbents at −196 °C, using the adsorption branch. The same models were applied to calculate mesopore volumes; the specific surface area was determined by Brunauer-Emmett-Teller (BET) method. Ultraviolet–visible diffuse reflectance spectroscopy (UV–Vis-DRS) was recorded with a Perkin Elmer Lamba 650 spectrophotometer equipped with a diffuse reflectance accessory. MAS-NMR spectra of ^{29}Si, ^{27}Al, ^{71}Ga and ^{51}V were recorded at room temperature on a Bruker MSL-300 spectrometer equipped with a 4-mm MAS probe. The spectrometer operated at 78.2 MHz for ^{27}Al. The samples were spun at the magic angle at a rate of 5 kHz. The spinning rate for all the samples was 10 kHz. Different numbers of scans were recorded for each compound in order to obtain an adequate signal to noise ratio. The recycling time was 4 s. The contact time during CP was 800 μs for B63 and 1.5 ms for the other compounds. The Si environment was studied at the resonance frequency of ^{29}Si (79.46 MHz). The samples were packed in a 4 mm zirconia rotor and measured with a spinning frequency of 8000 Hz. 4.14×10^6 scans were accumulated with a recycle delay of 6 s and a pulse length of 2.0 μs (30°). tetramethylsilane (TMS) was used as shift reference. The study of the Ga and V coordination was performed at the resonance frequency of ^{71}Ga (152.52 MHz) and ^{51}V (105 MHz), respectively. The samples were packed in a 3.2 mm chemagnetics rotor and measured with a spinning frequency of 12,000 Hz. 5×10^6 scans were accumulated with a recycle delay of 0.1 s and a pulse length of 1.2 μs (10°).

X-ray Photoelectron Spectra (XPS) were obtained on a MicrotechMultilb3000 spectrometer. The unmonochromatized AlKα X-ray source (1486.6 eV, 12 kV, 15 mA), with no charge neutralizer, was applied to generate core excitation. The system was calibrated according to ISO 15472:2001. The lower energy scan increases the absorption cross-section resulting in larger signal-to-noise ratio and allowing smaller features in peaks to be discerned. An estimated error of ±0.1 eV can be assumed for all measurements. The Shirley-type background subtraction was used to the spectra prior to fitting procedure where Voigt line shape i.e. Gaussian/Lorentzian functional (70:30) was applied. In order to measure binding energies the C 1s signal of the adventitious carbon was used as reference at 284.8 eV. All samples were previously degassed for 12 h under ultra-high vacuum (<1.3×10^{-6} Pa) prior to the analysis. The modified Auger parameter of Al (α′) was calculated using the following equation [36]: $\alpha' = 1253.6 + KE(Al_{KLL})$ - KE (Al 2p), where KE (Al_{KLL})) is the kinetic energy of the Auger electron of Al_{KLL} and KE(Al 2p) the kinetic energy of the photoelectron Al 2p. TEM were recorded in a JEOL 2100F microscope operated with an accelerating voltage of 200 kV (point resolution of 0.19 nm); coupled with energy-dispersive X-ray spectroscopy (EDS). Raman spectrum was obtained from an InVia Reflex Raman microscope and spectrometer using a 532 nm diode laser excitation. Before recording the spectra, the spectrometer was calibrated using the Raman band at 520 $cm^{-1}$of a standard SiO_2 sample. JASCO 5300 FTIR spectrometer was used for Py-FTIR measurements. A thermostated cell with a special NaBr window warmed up to 400 °C and 4.2×10^{-2} Torr during 2 h was employed to avoid possible sample hydration.

2.6. Catalytic activity

In this study the oxidation reaction of dibenzothiophene (DBT) was carried out in the L (acetonitrile as solvent) - S (catalyst) phase system in order to avoid the mass transfer effect and, thus, study the intrinsic rate of the catalysts themselves. Those limitations have been studied in our previous works [23,24] and the result of comparing the two different phase systems was that L–S system turned out in higher DBT conversions to sulfone than those in L–L–S system. The results indicate that mass transfer between the two liquid phases affects the overall sulfur removal rate, and hence, that a useful comparison of the activity of the various catalysts can only be made eliminating L–L mass transfer effects. Therefore, in this study we will use a two-phase system.

The catalytic oxidation of DBT with hydrogen peroxide (30 wt %) was carried out in a 100 mL glass batch reactor, equipped with a magnetic stirrer, a thermometer and a condenser. In a typical run, the solid catalyst (60 mg) was suspended under stirring (750 rpm) in 20 mL of a solution containing 500 ppm of S as DBT in acetonitrile. H_2O_2/DBT ratio was 6 (O/S = 12) at a constant temperature of 60 °C. To evaluate the conversion of DBT, a set of samples were recovered at various times and immediately analyzed qualitatively by gas chromatography (GC) HP 5890 Series II with HP-5 column and connected to FID and PFPD detectors. Sulfones were confirmed using a Shimadzu GCMS-QP5000 with a GC-17A gas chromatograph and AOC-20i autoinjector and HP-5 column 30-m length, 25-mm inner diameter, and 25-μm film thickness.

ODS of DBT was fitted by a pseudo-first order kinetic, where the rate constant (k) and reaction time (t) can be described using the following equation:

$$\ln(C_t/C_0) = -kt \quad (1)$$

where C_t is molar concentration at time t and C_0 is initial molar concentration.

The Arrhenius equation was used to calculate the activation energy:

$$k = A \exp(-Ea/RT) \quad (2)$$

where A is the pre-exponential factor, Ea is the apparent activation energy, and R and T are the gas constant and reaction temperature (K), respectively.

For the deactivation study, the catalysts used were regenerated by oxidative air treatment. First, the spent material was washed several times with excess amount of methanol and water and then filtered. The solid was dried and then calcined at 400 °C for 4 h ramped at 1.5 °C/min. After that, the sample was stored in a heater to avoid wetting before being tested in the next desulfurization cycle. The experimental conditions were the same as those described above. However, in this study, the amount of catalysts was lowered to 30 mg to avoid working at high conversion levels close to 100%.

3. Results and discussion

3.1. Characterization of the catalysts

3.1.1. XRD

Fig. 1(a) shows small angle X-ray diffraction pattern of pure SBA-15 and vanadium-modified VOx-SBA-15 (y). At the 2θ region between 0.9° and 2.0° we can observe the three typical peaks of (100), (110) and (200) reflections corresponding to 2D-hexagonal SBA-15 material (P6mm). The vanadium-modified samples presented a decrease in peak intensity and a shift to higher angle as vanadium content increased. This behavior might be attributed to the presence of vanadium oxide species anchored to the silica framework increasing wall thickness, in spite of the fact that the mesoporous structure was perfectly kept as the original SBA-15 support [35].

Fig. 1 (b) shows the wide angle XRD patterns of SBA-15 materials. The profiles are the typical ones for amorphous pore walls SBA-15 with a broad halo extending from 2<theta> 15 to 37° [37–41]. The samples with higher vanadium loading (1/5 and 1/10) shows diffraction peaks characteristic of crystalline V_2O_5 (JCPDF 65-0131of V_2O_5 characteristic peaks at ca. 2θ = 16, 22, 26 and 32° (supplementary files)) [42]. The absence of the peaks of V_2O_5 phase in the less loaded samples suggests that vanadium clusters are very small and highly dispersed over the support.

The XRD of V-SBA-15 (Fig. 2) shows that the pattern is very similar to SBA-15, indicating the success of the method of the synthesis. Crystalline pattern of V_2O_5 was not observed at wide angle (Inset). Fig. 3 shows XRD spectra of Al-SBA-15 and its vanadium counterparts. We observe that the structure was maintained after incorporation of aluminum. Subsequent vanadium modification only caused a slight disorder in structure, as the peak shifted to higher angle and intensity decreased. The inset shows that vanadium species are highly dispersed on this support. Fig. 4 shows the low-angle diffraction patterns of gallium-containing samples. We can observe that the incorporation of gallium does not produce changes in the SBA-15 mesostructure. When vanadium was incorporated into Ga-SBA-15, a behavior similar to that found in Al-SBA-15 support was shown, as mentioned before. In the inset of Fig. 4, we observe the wide-angle spectrum for VOx-Ga-SBA-15; no peaks of Ga_2O_3 were detected, probably due to the gallium species are very well dispersed into the framework. Also, the peaks of vanadium oxides are no clearly detected in the spectra, indicating good dispersion of the vanadium moieties.

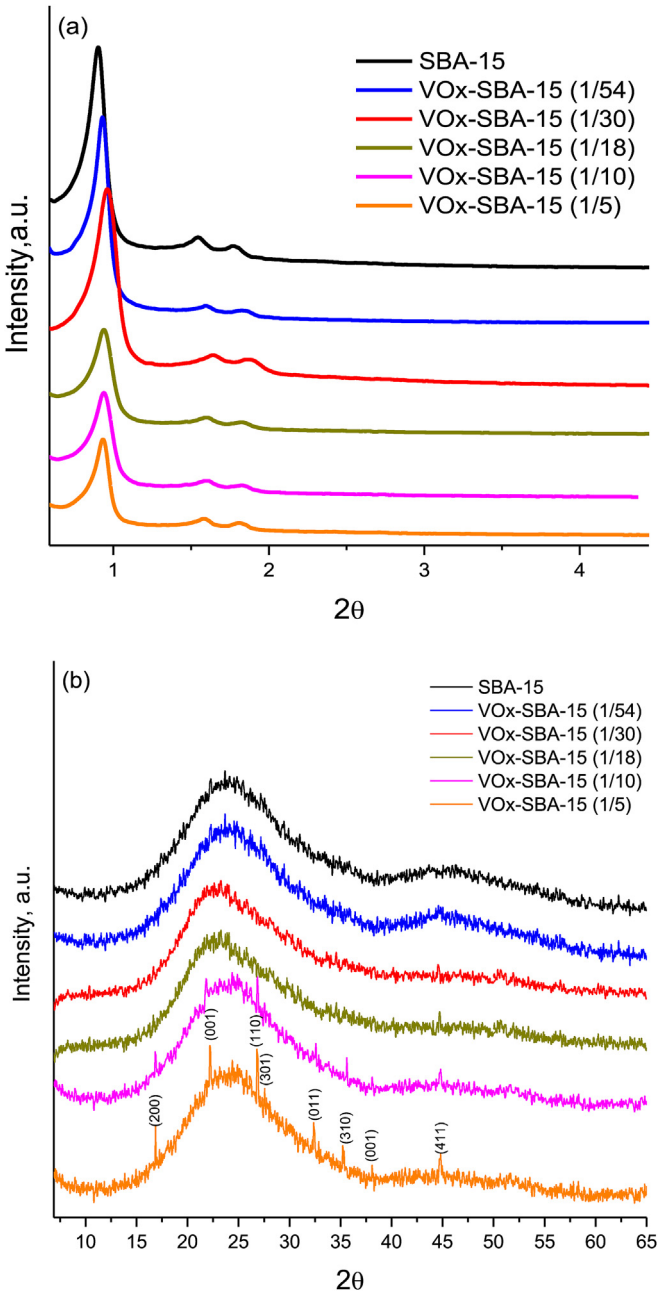

Fig. 1. XRD of VOx-SBA-15 with different V/Si ratios: (a) low angle and (b) wide angle.

3.1.2. N_2 adsorption-desorption isotherms

N_2 adsorption-desorption isotherms for VOx-SBA-15 samples with different vanadium loading are type IV isotherms with an H1 hysteresis loop, typical of the SBA-15 structure (Fig. 5). The curves exhibited a significant uptake at P/P_0 = 0.50–0.80 indicating capillary condensation within the mesopores. In the case of the more loaded sample (V/Si = 1/5), the atypical shape of the isotherm confirms the loss in structure when a high amount of vanadium is added to the mesoporous material. As can be seen in the inset of Fig. 5, the two cycles of hysteresis observed could be attributed to the formation of pores of higher size. The rest of the samples show a

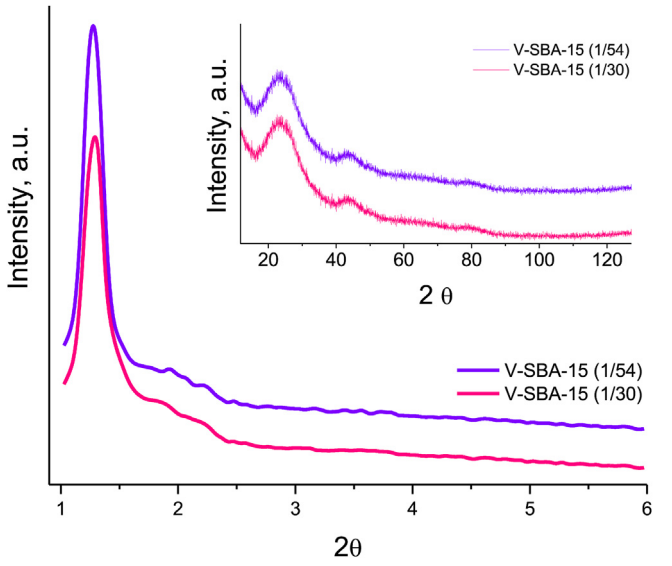

Fig. 2. Low angle XRD of V-SBA-15 with different V/Si ratios. Inset: wide angle XRD.

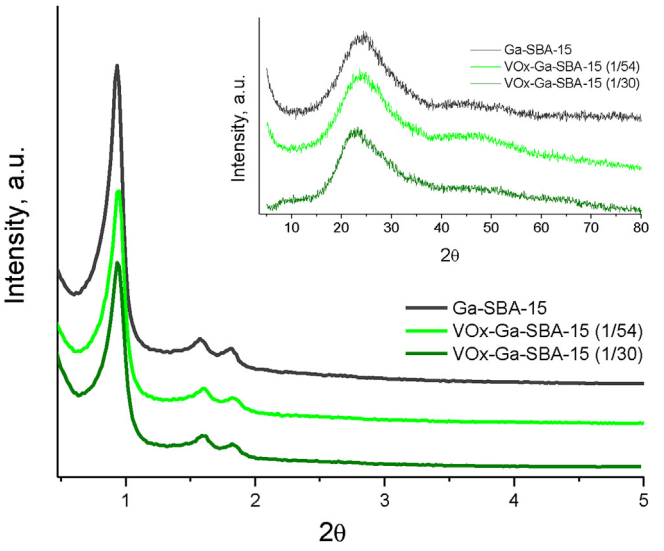

Fig. 4. Low angle XRD of VOx-Ga-SBA-15 with different V/Si ratios. Inset: wide angle XRD.

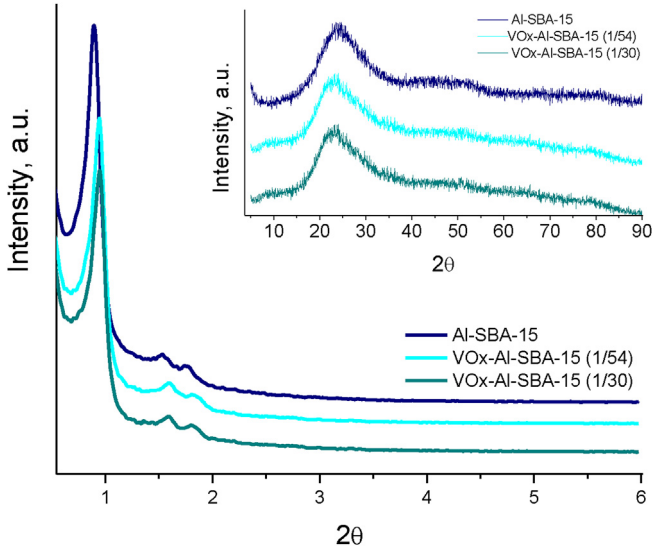

Fig. 3. Low angle XRD of VOx-Al-SBA-15 with different V/Si ratios. Inset: wide angle XRD.

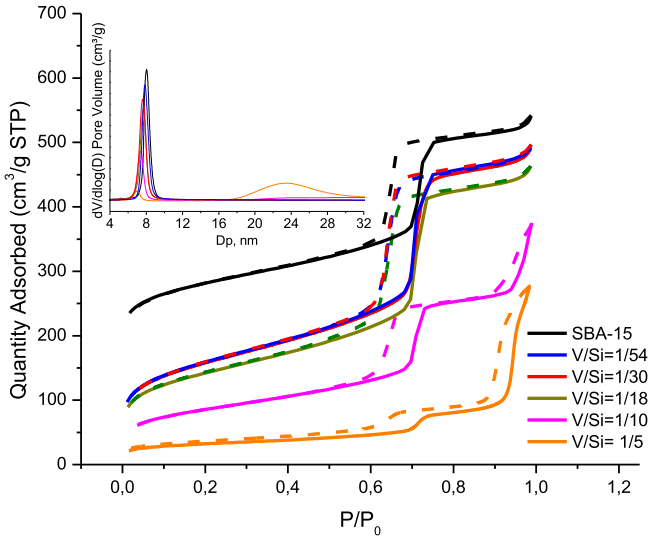

Fig. 5. (a) N_2 adsorption/desorption isotherms of VOx-SBA-15 (y) samples. Inset: pore size distribution.

narrow and uniform pore size distribution. Pore size decreases as vanadium content increases.

Fig. 6 shows nitrogen adsorption/desorption isotherms of V-SBA-15 material. The samples display type IV isotherms with an H1 hysteresis loop, demonstrating that the SBA-15 structure was obtained.

Figs. 7 and 8 show the isotherms of the modified supports with Al and Ga, respectively. Type IV isotherms with an H1 hysteresis loop were obtained in all cases, indicating that SBA-15 structure was maintained. The incorporation of vanadium presents a similar behavior to that observed when siliceous-SBA-15 support was used.

Table 1 provides the textural properties of the catalysts synthesized. We observe that the modification with vanadium in SBA-15 support causes a decrease in surface area, pore volume and pore size. This suggests that some of vanadium species are incorporated into the mesoporous channels. The specific surface area of the sample with high loading of vanadium (V/Si = 1/5) showed a dramatic loss of area indicating some pore blockage. In the samples with lower V/Si ratios (1/30 and 1/54), the mesoporous structure was maintained and the structural parameters obtained suggest that the vanadium species could be successfully incorporated into the pores.

In contrast, pore diameter had a marked increase when vanadium was introduced to the molecular sieves by direct synthesis. This fact indicates that vanadium atoms could be part of the framework replacing Si atom. The increase in pore diameter might be due to the longer bond length of V with oxygen than that of Si–O http://www.sciencedirect.com/science/article/pii/S0926860X16300850 [22]. The same occurred when Al or Ga were incorporated into the SBA-15 framework. The incorporation of the heteroatom diminished the SBET area; yet, in all cases, it still kept high compared with pristine SBA-15.

3.1.3. Al-SBA-15 MAS-NMR

In order to determine the location of the Al atom in the framework, NMR of Al-SBA-15 was performed. Fig. 9 (a) shows the

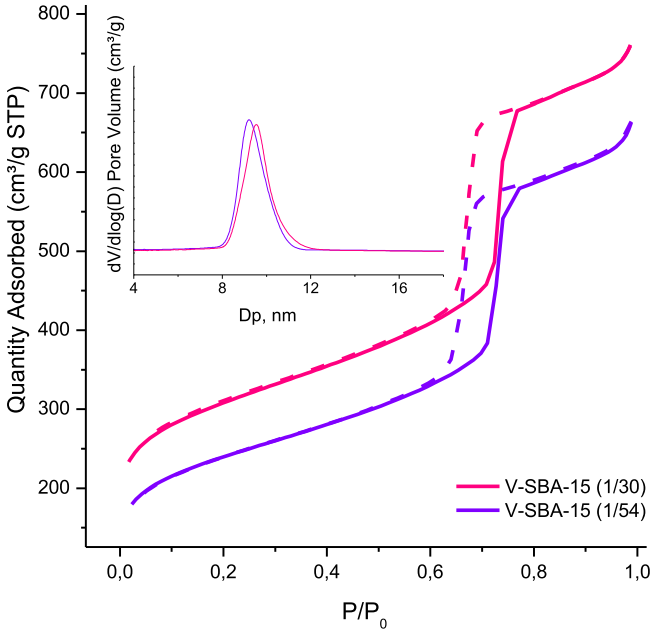

Fig. 6. (a) N_2 adsorption/desorption isotherms of V-SBA-15 (y) samples. Inset: pore size distribution.

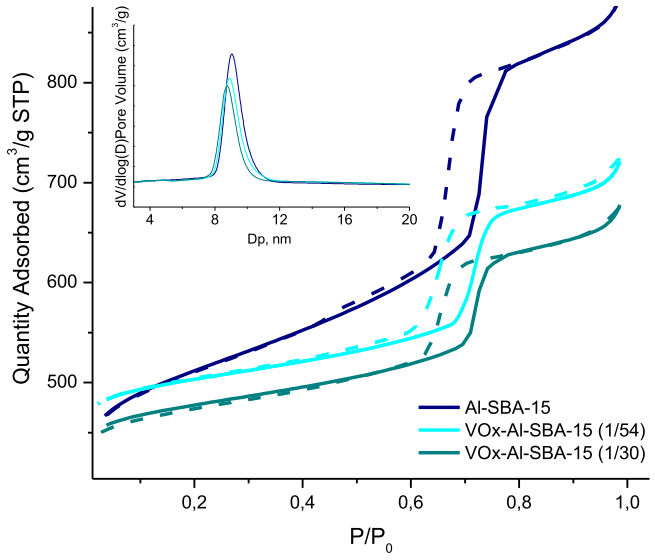

Fig. 7. (a) N_2 adsorption/desorption isotherms of Al-SBA-15 and VOx-Al-SBA-15 (y) samples. Inset: pore size distribution.

^{29}Si-MAS-NMR spectrum, where a prominent peak at −111 ppm is assigned to $[Si(OSi)_4]$ (Q4) and a lower signal at −101 ppm is assigned to $[Si(OSi)_3OH]$ (Q3) [43], indicating that the incorporation of Al by post-alumination did not disturb tetrahedral Si in the SBA-15 framework. The spectrum of ^{27}Al in Al-SBA-15 shown in Fig. 9 (b) exhibits a very intense signal at 50 ± 2 ppm assigned to tetrahedral-coordinated framework aluminum, indicative of Al in framework position.

3.1.4. Ga-SBA-15 MAS-NMR

The position of gallium in the SBA-15 sample was studied by ^{71}Ga-NMR spectroscopy http://www.sciencedirect.com/science/article/pii/S0926860X09005924 [44]. Fig. 9 (c) shows the spectrum of Ga-SBA-15, where one regular peak at 150 ppm is observed.

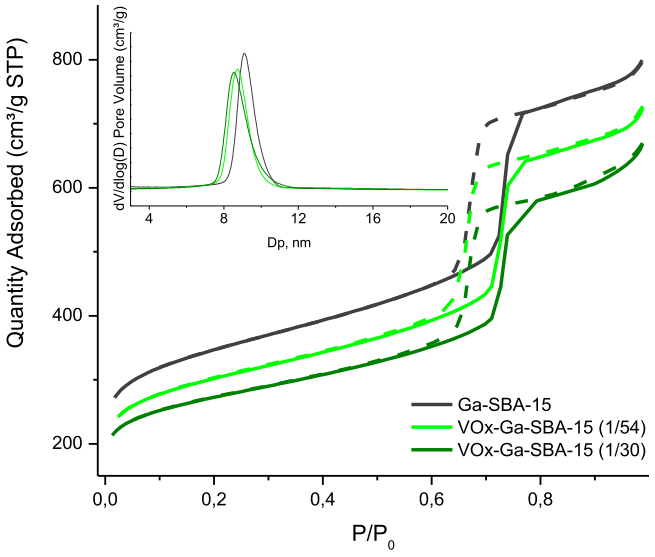

Fig. 8. (a) N_2 adsorption/desorption isotherms of Ga-SBA-15 and VOx-Ga-SBA-15 (y) samples. Inset: pore size distribution.

Table 1
Textural properties of the samples synthesized.

Samples	A (m^2/g)	V_p (cm^3/g)	D_p (nm)
SBA-15	1050	1.29	8.02
VO_x-SBA-15 (1/54)	702	0.90	7.78
VO_x-SBA-15 (1/30)	678	0.89	7.70
VO_x-SBA-15 (1/18)	616	0.85	7.56
VO_x-SBA-15 (1/10)	340	0.68	7.41
VO_x-SBA-15 (1/5)	132	0.49	6.84
V-SBA-15 (1/54)	965	0.99	9.13
V-SBA-15 (1/30)	845	0.94	9.59
VOx-Al-SBA-15 (1/54)	825	1.06	8.89
VOx-Al-SBA-15 (1/30)	796	1.03	8.77
VOx-Ga-SBA-15 (1/54)	762	1.12	8.81
VOx-Ga-SBA-15 (1/30)	704	1.01	8.50

V_P: Total pore volume; A: BET surface area; D_P: Pore diameter determined by NLDFT method from the adsorption branch.

This peak was assigned to gallium in tetrahedral coordination in agreement with the literature [45,46]. Fig. 9 (c) also shows a peak at 0 ppm, assigned to Ga atoms in octahedral position. The peak at 0 ppm corresponds to Ga_2O_3 [44,45].

3.1.5. V-SBA-15 MAS-NMR

Vanadium species in calcined V-SBA-15 have low anisotropy and asymmetry values in MAS-NMR studies [47–51]. Fig. 9 (d) shows the presence of vanadium species as V^{5+} consisting of a resonance at −450/−480 ppm, which can be attributed to distorted isolated tetrahedral V^{5+} of type V═O-$(SiO)_3$ in dehydrated catalysts, in agreement with V-containing mesoporous catalysts [50,51]. It is important to note that octahedral coordination of V ions was not detected in this sample (chemical shift around 300 ppm). In this region, a perpendicular component of an axially anisotropic spectrum of V_2O_5 can be detected at very low concentrations. Thus, most of the incorporated V is substituted into the silica framework in tetrahedral coordination with surrounding oxygen anions.

3.1.6. TEM

Fig. 10 shows the TEM of the samples with V/Si = 1/30. They present the typical hexagonal array with longitudinal channels corresponding to SBA-15 mesoporous material. Vanadium clusters

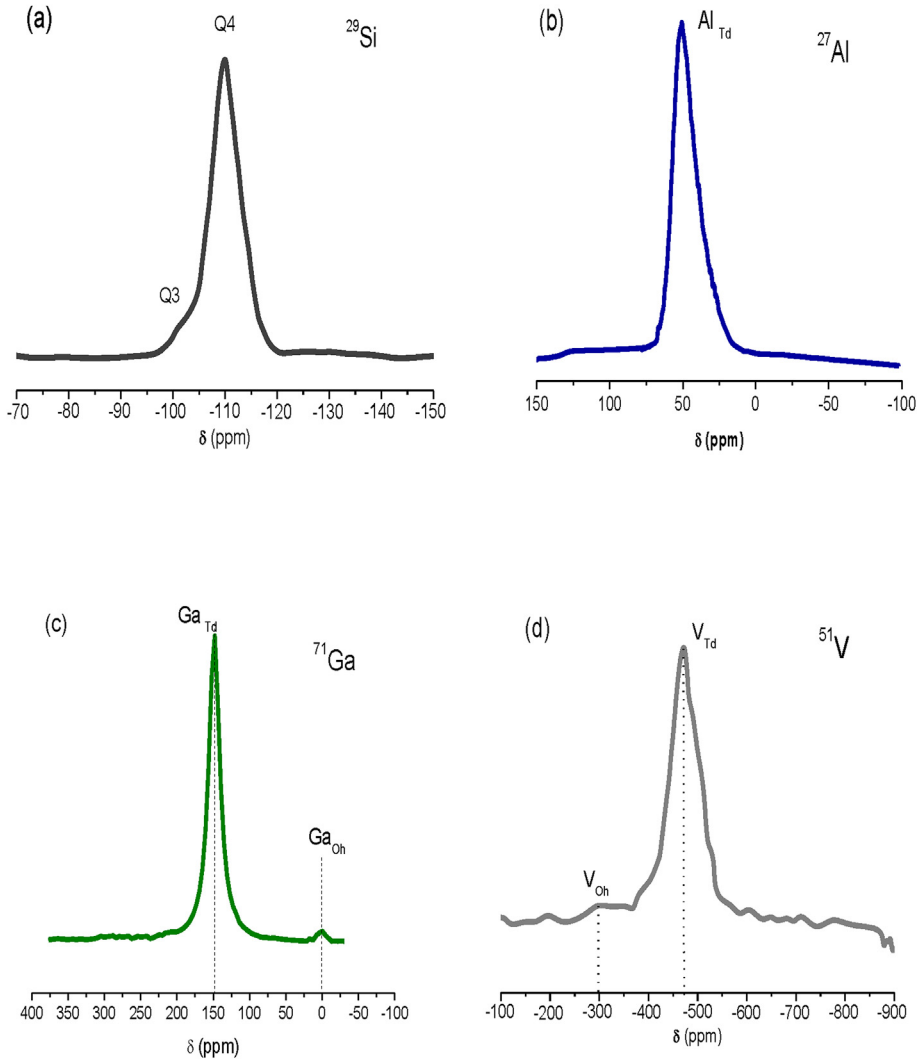

Fig. 9. (a) ^{29}Si and (b) ^{27}Al-MAS-NMR spectrum of Al-SBA-15, (c)^{71}Ga-MAS-NMR spectrum of Ga-SBA-15, (d) ^{51}V-MAS-NMR spectrum of V-SBA-15 (1/30).

are not visible in the images, probably due to the good dispersion and their very low size.

The images demonstrate that the structure remained after the metal (V, Ga, Al) incorporation. More images were added as supplementary file.

3.1.7. UV–vis-DRS

UV–Vis diffuse reflectance spectroscopy spectra give additional structural information on the surface VOx species, the energy of the oxygen-vanadium charge transfer bands indicating the coordination of the V center [52]. According to the literature [53–65], the structures of dehydrated VOx species mainly include isolated tetrahedral VO_4 species, oligomer pseudo-tetrahedral VOx species, polymeric octahedral VOx species and bulk V_2O_5 microcrystal.

In this work UV–Vis- DRS was used to study the dispersion and chemical environment of vanadium incorporated in the SBA-15 support. The results are shown in Fig. 11. The SBA-15 support exhibited only a very low intensity spectrum (not shown). Fig. 11 (a) displays the spectra of VOx-SBA-15 samples with different V/Si ratios.

The band with a maximum at 240 nm corresponding to low-energy charge transfer (CT) transitions between tetrahedral oxygen ligands and isolated V^{5+} cations assigned to isolated tetrahedral V^{5+} sites [52,56–62,66,67] is absent in these samples.

In this case, all the samples show a broad absorption band centered between 250 and 300 nm. It has been reported [62] that the band maximum of the charge transfer (CT) transitions of V^{5+} shifts to higher wavelength with increasing coordination number and that the oligomerization of tetrahedral V^{5+} is only evidenced by a broadening of the absorption bands and/or a small shift of the absorption maximum to lower energy (higher wavelength). The observed shift to slightly higher wavelength (260–270 nm) indicates the increase in the coordination number evidencing oligomerization of VOx species (Fig. 11 (a)). The other CT band centered at ~350–400 nm can be attributed to the presence of polymeric octahedral VOx species [57,58]. The intensity of the bands increases with the increase in vanadium loading. It should be noted that band intensity at 260–270 nm is significantly higher than that at 350–400 nm, indicating that a high proportion of pseudo-tetrahedral or oligomerized tetrahedral VOx species are present in all the samples. In addition, for VOx-SBA-15 samples with the higher vanadium loading, the broadening of the band suggests the formation of aggregated VOx chains [53,58] as V_2O_5 nanocrystals on the surface of the support. This is in agreement with previous wide angle XRD characterization.

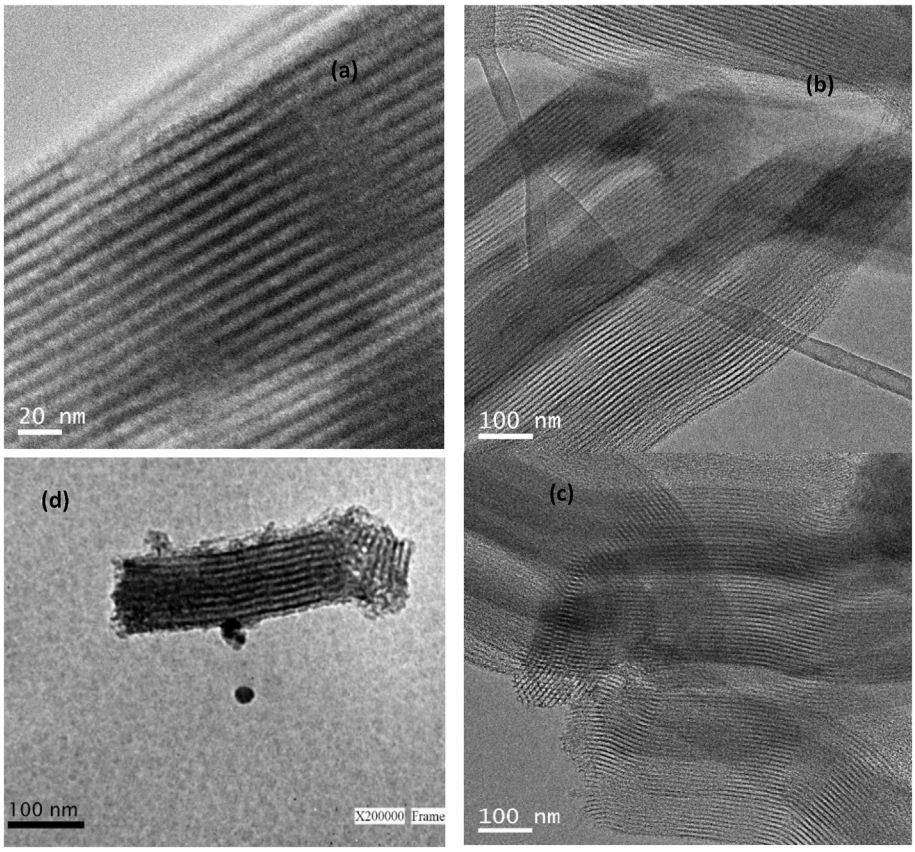

Fig. 10. TEM images of: (a) VOx-SBA-15 (1/30) (b) V-SBA-15 (1/30) (c) VOx-Al-SBA-15 (1/30) (d) VOx-Ga-SBA-15 (1/30).

Fig. 11(b) shows the spectra for V-SBA-15 samples. We observe a band with a maximum at 240 nm assigned to the isolated V^{5+} sites, where the species are in pseudo-tetrahedral symmetry as V═O $(Si{-}O)_3$, the presence of this tetrahedral V═O isolated monomeric VO_4^{3-} has been reported for similar systems http://www.sciencedirect.com/science/article/pii/S2095495616300390 [56–61]. Both samples show a shoulder at higher wavelength indicating the presence of some oligomeric tetrahedral V^{+5} species. The results are in agreement with the previous characterization that indicates that vanadium is mainly an isolated tetrahedral species.

Fig. 11 (c) shows the spectra for VOx-Ga-SBA-15 and VOx-Al-SBA-15 samples. In these spectra, the band with a maximum at ~240 nm assigned to the isolated tetrahedral V^{5+} sites appears in all the samples and with high intensity. This fact indicates that the incorporation of Al or Ga further improves vanadium dispersion. The tetrahedral isolated vanadium is the predominant species in these catalysts, with the exception of VOx-Al-SBA-15 (1/30) sample, where some vanadium oligomeric species are also present. In addition, the band centered at 500 nm indicating the presence of polymerized VOx species or bulk-like V_2O_5 due to a further polymerization of VOx species was not observed. This is in agreement with wide-angle XRD results.

Similar UV–Vis features observed with other impregnated V-SBA-15 systems [56,66] were ascribed to the presence of vanadium aggregates along with isolated sites.

In Fig. 11 (a) and (c) we observe that the presence of Ga and/or Al in the support slightly shifts the bands to lower wavelength indicating the presence of isolated vanadium species, this fact gives account of the higher dispersion of the vanadium species.

Given these results, it is clear that the nature of VOx species is closely related to preparation methods, vanadium loading and structure and nature of the support.

3.1.8. XPS

Fig. 12 shows the $V2p_{3/2}$ core level spectra in the VOx-SBA-15 samples with different V/Si ratios. The only contribution observed in all the samples was at 517.2–517.5 eV. According to the literature, the 517 eV signal is assigned to V^{5+} in the form of V_2O_5. The contribution centered about 516.3 eV attributed to V^{4+} species was not observed [63,64]. The contribution at about 532 eV is due to the oxygen from silica. In addition, the contribution at low binding energy (530.1 eV) is derived from V_2O_5 [68–70].

An exact determination of the V2p binding energy of vanadium species of V-SBA-15 (not shown) was difficult since XPS is a surface technique and vanadium mainly could be incorporated deep inside the channels of SBA-15, high dispersion and low concentration of vanadium species on the surface may contribute to its weak signal intensity [70–73].

The binding energy (BE) of $Ga2p_{3/2}$ (Fig. 13 (a)) and $Al2p_{3/2}$ (Fig. 14 (a)) appears at 1118.7 eV and 74.6 eV, respectively [73]. Accordingly, the value of 74.6 eV for BE indicates that the Al phase of the Al-SBA-15 materials can be assigned to AlxOy (x/y = 3:1 or 1:1), where Al is less oxidized than Al_2O_3 [74]. In order to determine the chemical environment of Al we studied the Auger parameter (α'). This parameter is independent of the sample charging but allows us to determine the tetrahedral or octahedral coordination. Thus, α' lower than 1460.4 eV are characteristic of tetrahedral Al, whereas α' values higher than 1461.0 eV are characteristic of octahedral Al [36,74–76]. Fig. 14 (b) shows the Al $_{KLL}$ spectra for the Al-SBA-15, only one signal around 1385 eV was observed. The

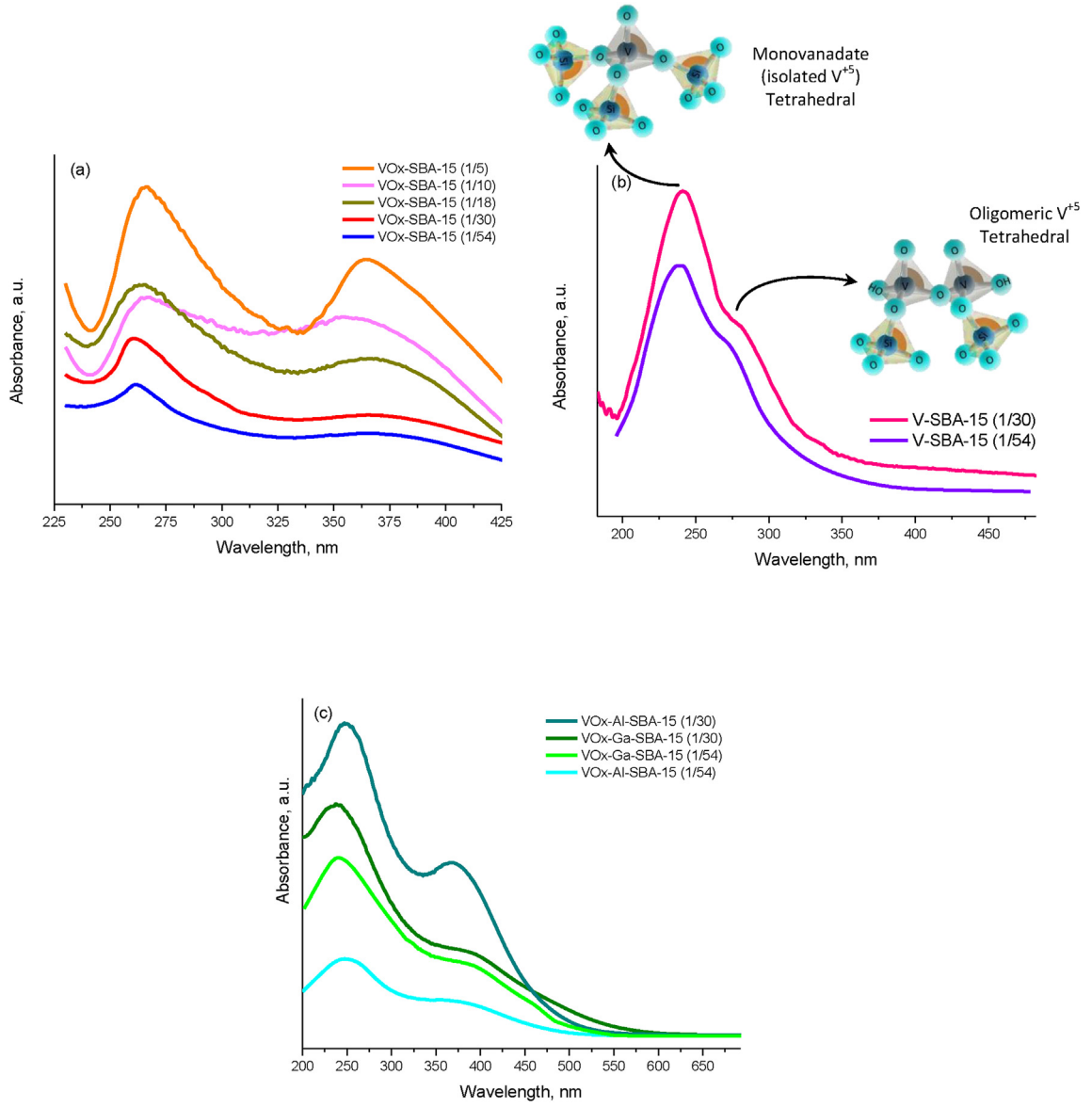

Fig. 11. UV–Vis diffuse reflectance spectra of (a) VOx-SBA-15 (y), (b) V-SBA-15 (y), (c) VOx-Ga-SBA-15 (y) and VOx-Al-SBA-15 (y).

Auger α' parameter calculated using the KE of the peak was 1458.2, which is characteristic of the framework tetrahedral aluminum.

In Fig. 13 (b) and 14 (c) we assume that V species correspond to V^{+5} as V_2O_5. These analyses are in agreement with MAS-NMR studies and UV–Vis-DRS.

Table 2 shows the atomic Metal/Si ratio obtained by XPS in all samples. The low ratios found by XPS indicate that most vanadium species are in the inner surface of the mesoporous support. Likewise, Al and Ga species are mainly dispersed in the internal surface of the support since the ratios are very low (especially Ga/Si less than 0.003). Table 2 also shows the wt.% of vanadium in the samples obtained by EDS.

3.1.9. TPR

To investigate the reducibility of vanadium species dispersed on the support, the TPR profiles of the catalysts are comparatively depicted in Figs. 15 and 16.

Fig. 15 shows the TPR profile of VOx-SBA-15 (y) samples. There is one reduction peak for all catalysts, assigned to the reduction of V^{5+} [77–82]. Peak temperature is centered at 556–562 °C. The sample with the lowest V loading presents the lower reduction

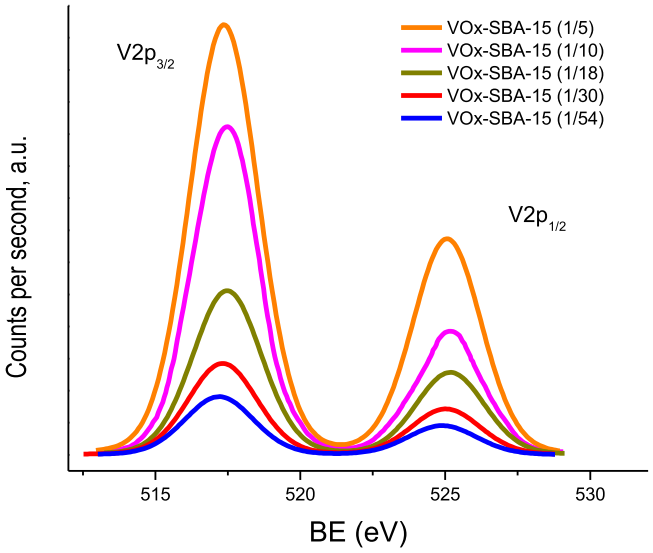

Fig. 12. XPS of VOx-SBA-15 (y) samples.

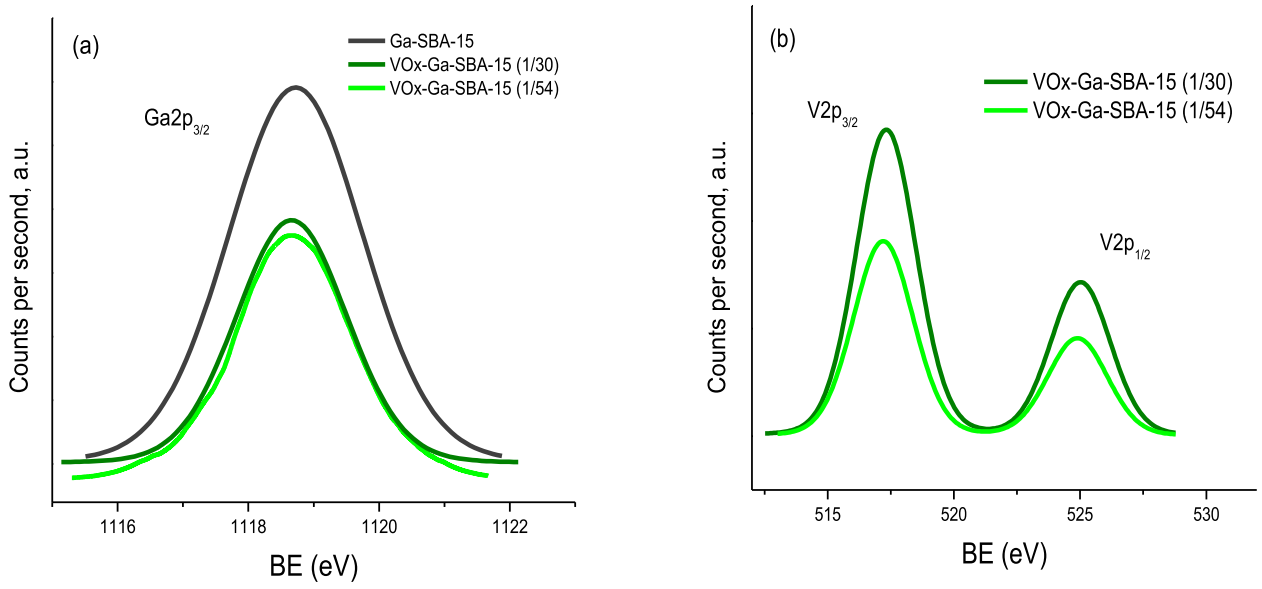

Fig. 13. XPS of VOx-Ga-SBA-15 (y) samples (a) BE of Ga and (b) BE of VOx.

temperature of 556 °C, attributed to the reduction of dispersed tetrahedral vanadium species or low oligomeric V–O–V groups. For the most loaded VOx-SBA-15(1/5) sample, the peak is shifted to a higher temperature of 562 °C, suggesting that the formation of V_2O_5-like polymeric vanadium species at high vanadium loading (determined by UV–Vis-DRS) will slightly retard the reduction of V^{5+} [70].

Fig. 16 shows the TPR of VOx-Ga-SBA-15 (y), VOx-Al-SBA-15 (y) and V-SBA-15 (y) samples. VOx-Ga-SBA-15 samples show peak maxima at 508 °C, while VOx-Al-SBA-15 samples, peak positions shift towards a higher temperature of 567 °C.

The lower reduction temperature in VOx-Ga-SBA-15 corroborates the presence of well-dispersed tetrahedral vanadium species on VOx-Ga-SBA-15 compared with VOx-Al-SBA-15 and VOx-SBA-15 catalysts, which may get easily reduced, while the formation of higher vanadate species shifts the peak maximum to higher temperatures in VOx-SBA-15 catalysts. In VOx-Al-SBA-15 samples, the reduction peaks occur at slightly higher temperatures than those in VOx-SBA-15, probably due to a higher metal-support interaction present in a more acid support, generated by the tetrahedral aluminum in the framework. These results are in agreement with those of previous studies reporting that higher reduction peak temperatures are indicative of stronger metal-support interactions [83,84].

Fig. 16 also shows TPR of V-SBA-15; the lowest reduction temperature (411 °C) agrees with the well-dispersed tetrahedral vanadium species on V-SBA-15 catalyst, which may get easily reduced.

George et al. [70] determined the average oxidation state values for V-MCM-41 and grafted V/MCM-41 at 4.5 and 3.5, respectively, showing that reduction of V was more pronounced in the grafted catalysts than in the vanadium-incorporated mesoporous catalysts. That could explain the differences in the nature of the profiles obtained.

3.1.10. Raman

The type of V species formed on the surface of the SBA-15 was studied by Raman spectroscopy. Raman spectroscopy has a higher sensitivity to the presence of oxide-like species than XRD [85]. Fig. 17 shows the Raman spectra for the samples with better textural and structural properties. As shown in Fig. 17, the samples show bands corresponding to different vanadium species present on the surface. We observe, a band at ~1036 cm^{-1}, which is the defining characteristic of the tetrahedral V=O stretching vibration in isolated monomeric VO_4^{3-} species [25,86–89]. This band is more prominent in VOx-Ga-SBA-15 and VOx-Al-SBA-15, indicating the presence of tetrahedral isolated monomeric VO_4^{3-} species as mainly species in these samples. In addition, the weaker vibrational modes at 930 cm^{-1} are assigned to the V = O symmetric stretching of polymerized surface VOx species [90,91] also present in VOx-Ga-SBA-15 and VOx-Al-SBA-15 samples, which is consistent with the results of UV–Vis spectra. In the case of the samples VOx-SBA-15 (1/30 and 1/54), the intensity of the 1036 cm^{-1} band decreases and those belonging to polymeric species (996, 930, 698, 479 and 285 cm^{-1}) intensify [25,82,87,88,92]. This study confirms that the presence of aluminum but mainly gallium in the framework allows better dispersion of the vanadium active species, in this case isolated tetrahedral VO_4^{3-} species. The results are in line with UV–Vis-DRS results. Additionally the Ga-containing samples shows peaks of low intensity at 345, 416, 658 and 764 cm^{-1} related to the Ag optical modes of the β-Ga_2O_3 crystallites [93–95], confirmed the ^{71}Ga-MAS-NMR analysis.

3.1.11. Py-FTIR

The acid strength of the supports was studied using the Pyridine adsorption method. Py-FTIR spectra of the samples were measured in the region of 1700–1400 cm^{-1}. According to literature, pyridine adsorbed on Lewis acid sites exhibits signals at 1450, 1596 and 1615 cm^{-1} [96]. Bands at 1540 and 1640 cm^{-1} are assigned to Bronsted acid sites present in the material. Further, pyridine co-adsorbed on both Bronsted and Lewis acid sites gives rise to a band at 1495 cm^{-1} [97]. The quantification of Bronsted and Lewis sites is shown in Table 3. The results reveal the existence of only Lewis acid sites on the mesoporous silica. Density of Lewis sites disappears after outgassing at a very low temperature (100 °C) in SBA-15. A higher temperature, above 200 °C and 300 °C, is needed to completely remove the pyridine adsorbed on Lewis acid sites for the samples containing gallium and aluminum, respectively. The Py-FTIR study of the Ga-SBA-15 and Al-SBA-15 samples also shows Bronsted acid sites, which are even observed at 200 °C and 300 °C.

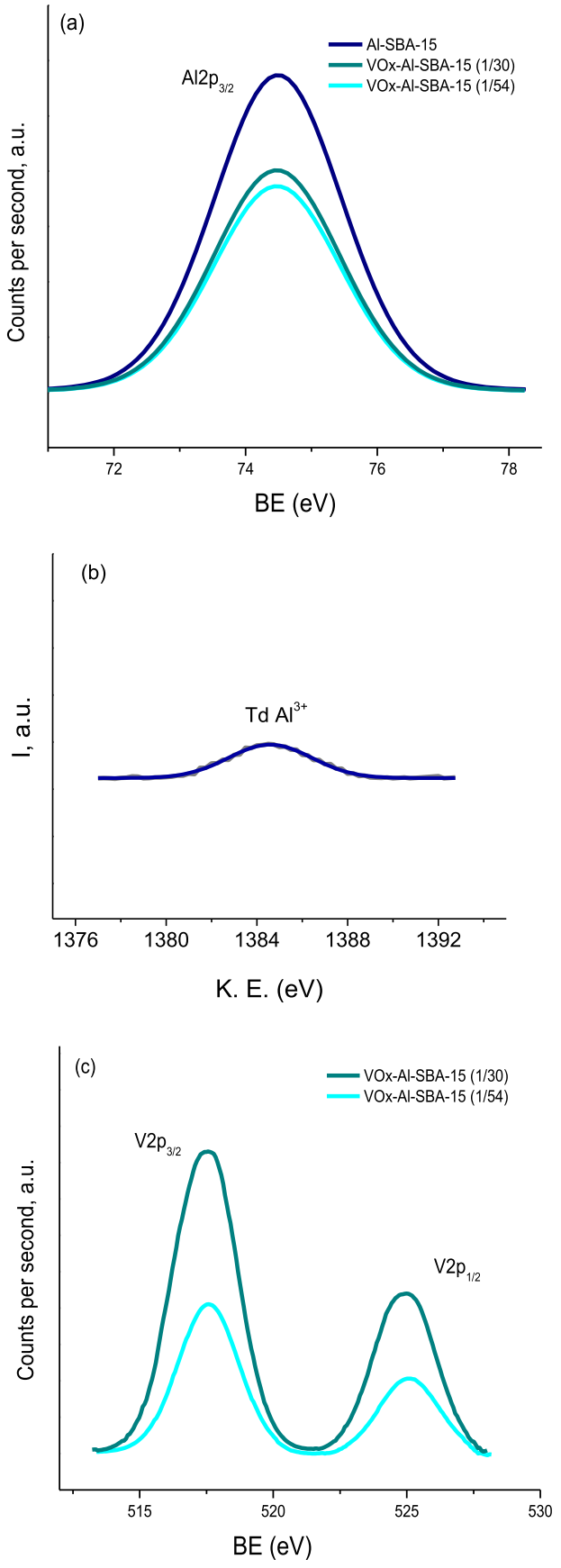

Fig. 14. XPS of VOx-Al-SBA-15 (y) samples (a) BE of Al, (b) Al $_{KLL}$ spectra and (c) BE of VOx.

The presence of pyridine molecules adsorbed at this temperature indicates the presence of acid sites at least with moderate strength. We can assume that the incorporation of Ga and Al gives rise to a small amount of moderate strong Bronsted acid sites.

3.2. Catalytic activity

The oxidative desulfurization of sulfur compounds occurs in a three-phase liquid-liquid-solid (L (oil) −L (solvent) −S (catalyst) system. In this process, the elimination of sulfur occurs by simultaneous extraction/oxidation of the S-molecule in the solvent solution, where is the catalyst and the oxidizing agent. The oxidizing agent interacts with the catalyst to produce large amounts of superoxide radical capable of oxidizing S-molecules in the solvent phase to their corresponding sulfones. After that, polar sulfones do not migrate to the oil phase. The catalytic cycle can be performed repeatedly under low temperature. In some cases, the transfer rate of S-compound from the oil phase to the solvent phase can affect the rate of the global process.

In order to avoid mass transfer limitations, the study of the intrinsic rate of the catalysts was performed in the two-phase liquid-solid (L (solvent) −S (catalyst) system. Fig. 18 shows the catalytic results from the ODS of DBT using VOx-SBA-15 catalysts with different V/Si in a (L−S) phase systems using acetonitrile as solvent and hydrogen peroxide as oxidant. DBT was selective to sulfone; sulfoxide or other products were not detected in the conditions studied. From the Figure, we can note that at 10 min of reaction time, VOx-SBA-15 with V/Si = 1/30 displays a DBT conversion of almost 100%. The samples with higher content of V showed lower activity.

According to the characterization techniques, VOx-SBA-15 (1/30) has a high proportion of isolated pseudo-tetrahedral VO_4^{-3} species. The presence of these well-dispersed isolated species would be responsible for the high activity in the ODS of DBT in the conditions studied. In addition, the lower activity obtained with the more loaded VOx-SBA-15 (1/5) sample shows that the aggregated VOx chains as V_2O_5 microcrystals are the less active species for this reaction. The activity decreased as follows: VOx-SBA-15 (1/30) >VOx-SBA-15 (1/54) >VOx-SBA-15 (1/18) >VOx-SBA-15 (1/10) >VOx-SBA-15 (1/5). The higher activity of VOx-SBA-15 (1/30) compared with VOx-SBA-15 (1/54) could be attributed to a higher vanadium content that supplies more isolated catalytic centers in VOx-SBA-15 (1/30). But the lower catalytic activity obtained with the incorporation of higher V/Si ratio may be related to the agglomeration of the vanadium species on the catalyst surface and a decrease in the amount of subsurface oxygen species.

Fig. 19 shows the activity of the catalysts modified with V, Al and Ga as heteroatom. The activity decreased as follows: VOx-Ga-SBA-15 (1/30) >VOx-Al-SBA-15 (1/30) >VOx-Ga-SBA-15 (1/54) >VOx-SBA-15 (1/30) > VOx-Al-SBA-15 (1/54) > V-SBA-15 (1/30) > V-SBA-15 (1/54). The catalysts modified with gallium and aluminum were the most active with total S-removal 95−99% at very short time. The optimal V/Si was 1/30. Isolated tetrahedral gallium incorporated in the inner surface of SBA-15 modified the nature of vanadium species and the interaction with SBA-15-type support, leading to a more homogeneous distribution of vanadium than in the other pure silica support. The dispersion of vanadium species is still high with the incorporation of aluminum in the SBA-15 support, since aluminum atoms serve as anchoring sites by strong interaction with V-species. SBA-15 sample is a weak Lewis solid acid catalyst in comparison with mesoporous silica of Al-SBA-15.

The modification of the support with Ga and Al had significant influence on the vanadium species state, dispersion and size. According to the characterization results, a large number of highly dispersed V-species are formed after the addition of Ga and/or Al.

Table 2
Core-level binding energies (eV) and surface atomic ratios of the samples.

Samples	$Si2p_{3/2}$	O1s	$V2p_{3/2}$	$Al2p_{3/2}$	$Ga2p_{3/2}$	Al/Si atom	Ga/Si atom	V/Si atom	V (wt.)[a]
VOx-SBA-15 (1/5)	103.4	530.1 (10) 532.8 (90)	517.4					0.1710	9.5
VOx-SBA-15 (1/10)	103.4	530.1 (5) 532.8 (95)	517.5					0.1240	5.7
VOx-SBA-15 (1/18)	103.4	530.1 (3) 532.8 (97)	517.5					0.0480	3.4
VOx-SBA-15 (1/30)	103.4	532.8	517.3					0.0240	2.2
VOx-SBA-15 (1/54)	103.4	532.8	517.2					0.0160	1.2
V-SBA-15 (1/30)									0.8
V-SBA-15 (1/54)									0.6
VOx-Al-SBA-15 (1/30)	103.3	532.7	517.5	74.6		0.007		0.0468	2.4
VOx-Al-SBA-15 (1/54)	103.3	532.7	517.5	74.6		0.004		0.0142	1.4
VOx-Ga-SBA-15 (1/30)	103.4	532.7	517.3		1118.7		0.003	0.0412	2.6
VOx-Ga-SBA-15 (1/54)	103.4	532.7	517.2		1118.6		0.002	0.0133	1.5

[a] EDS.

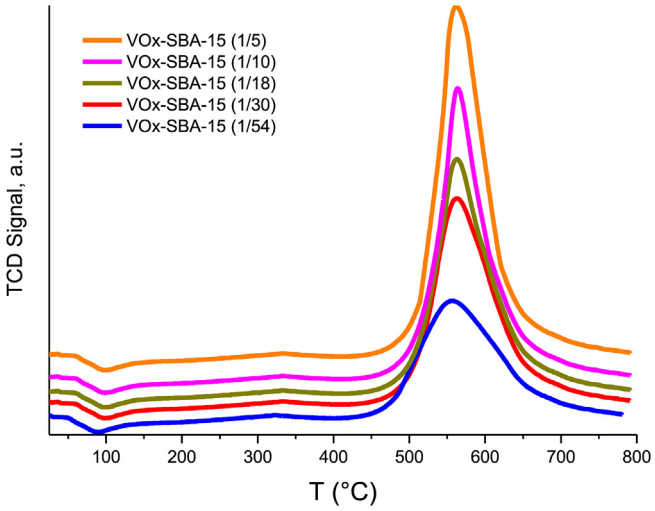

Fig. 15. TPR of VOx-SBA-15 (y) samples.

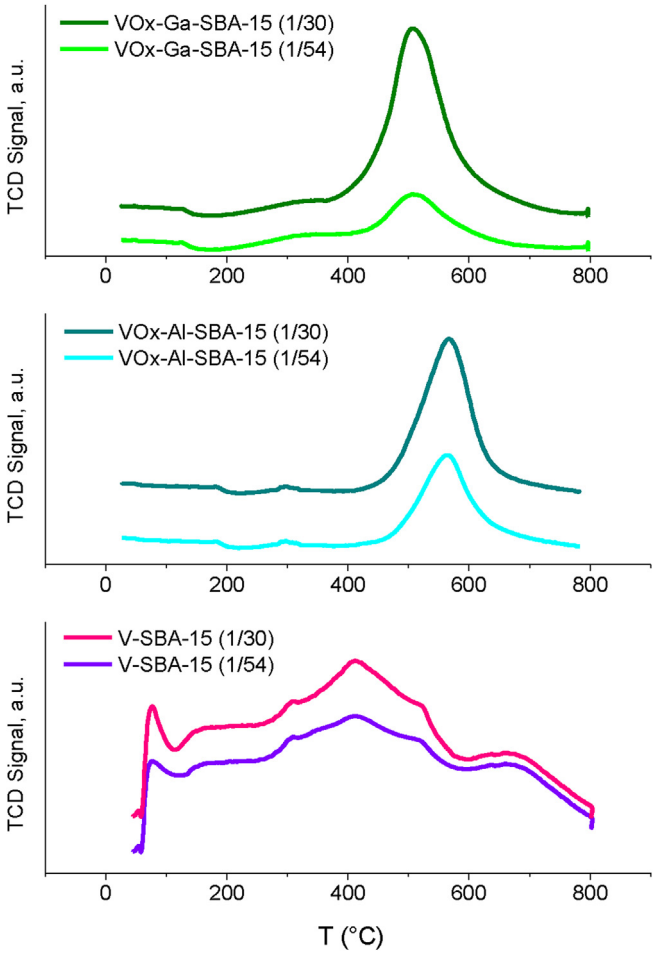

Fig. 16. TPR of VOx-Ga-SBA-15 (y), VOx-Al-SBA-15 (y) and V-SBA-15 (y) samples.

The tetrahedral position of Ga or Al resulted in the formation of a large number of highly dispersed VO_4^{-3} isolates species and thus the enhancement of the activity. Therefore, the catalytic activity for DBT oxidation is related to Ga and/or Al coordinated environment in the silica. Again, the higher activity of VOx-Ga-SBA-15 (1/30) compared with VOx-Ga-SBA-15 (1/54) could be due to higher vanadium-exposed catalytic sites in the more loaded sample (1/30). Is important to note that these samples also possess high surface area and pore volume, despite of the modifications. Surface area of more than 700 m^2/g could also be responsible for the good dispersion of vanadium and the better activity.

On the other hand, lower activity was found when vanadium was incorporated via direct synthesis in V-SBA-15. Even when vanadium was well dispersed, as mainly isolated species, in the high area support, the low vanadium content (0.8 wt% for V/Si = 1/30 sample and 0.6 wt% for V/Si = 1/54 sample) determined by EDS or inaccessible location of the active sites for the reactants could be ascribed to their low activity. However, a previous report by Shiraishi et al. [20] found that V-HMS in the ODS of Light Oil showed a higher activity than that in Ti-HMS; yet, at the same time, it consumed a higher quantity of H_2O_2. They concluded that the active species on vanadosilicate are radical species (V^{IV}–O–O*) formed by reaction with H_2O_2. In our case a further study on the method of the direct incorporation of vanadium into the mesoporous structure and a profound characterization of this catalyst is required to explain the lower activity.

The good activity of VOx-Ga-SBA-15 and VOx-Al-SBA-15 also could be related with the higher acidity of these supports compared with bare silica SBA-15 support.

Al incorporation creating acid sites that allow better anchorage of the catalytic species on the modified surface was studied in the oxidation of CO [32,33]. Gracia et al. [34] compared the activity of gallium and aluminum SBA-15 in the Friedel-Crafts alkylation of

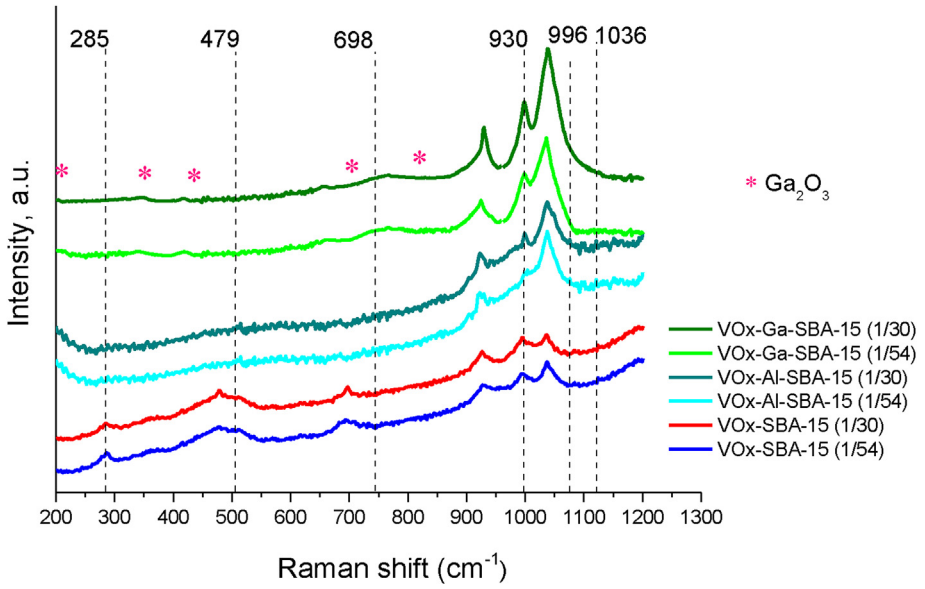

Fig. 17. Raman of VOx-Ga-SBA-15 (y), VOx-Al-SBA-15 (y) and VOx-SBA-15 (y) samples.

Table 3
Quantification of Bronsted and Lewis sites at different temperatures.

T (°C)	SBA-15		Ga-SBA-15		Al-SBA-15	
	B (mmol/g)	L (mmol/g)	B (mmol/g)	L (mmol/g)	B (mmol/g)	L (mmol/g)
50	–	0.32	0.12	0.41	0.29	0.59
100	–	0.17	0.10	0.19	0.13	0.25
200	–	0.00	0.08	0.02	0.10	0.15
300	–	0.00	0.00	0.00	0.04	0.10

toluene. They observed an increase in the Lewis acidity with an increase in the gallium content and an increase in Bronsted acidity with the incorporation of Al. The mesoporous Ga-SBA-15, with a higher contribution of Lewis acid sites, were highly active and selective in the liquid-phase alkylation of toluene with benzyl chloride. Al-SBA-15 materials, with a greater proportion of Bronsted acid sites, had an improved activity in the alkylation of toluene with benzyl alcohol.

In our case, according the pyridine FTIR characterization results shown in Table 3, the good activity can be attributed to the very good dispersion of the vanadium catalytic centers and to the synergic effect of Lewis and Bronsted acid sites, derived from Ga or Al incorporation. The effect of the support was changing the electronic environment of the vanadium sites due to the stronger interaction metal-support. In addition, we suppose that the acid centers could we involve in the mechanism of the reaction. This indicates that the trivalent heteroatom incorporation enhances the ODS activity or prevent the irreversible adsorption of the sulfones over the active centers.

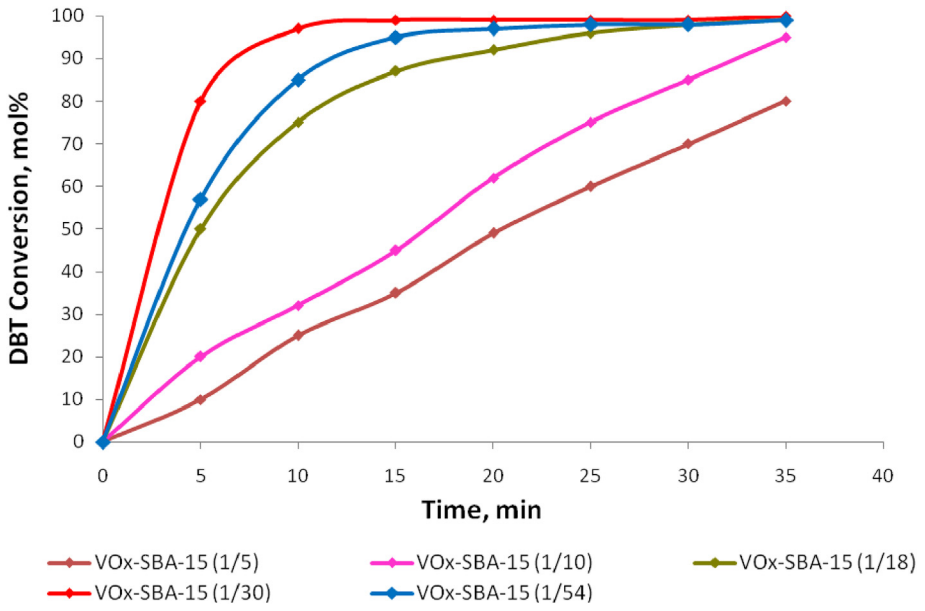

Fig. 18. Catalytic activity of VOx-SBA-15 (y) samples. Molar ratio O/S = 12, T = 60 °C. g DBT/g cat = 0.96 (500 ppm).

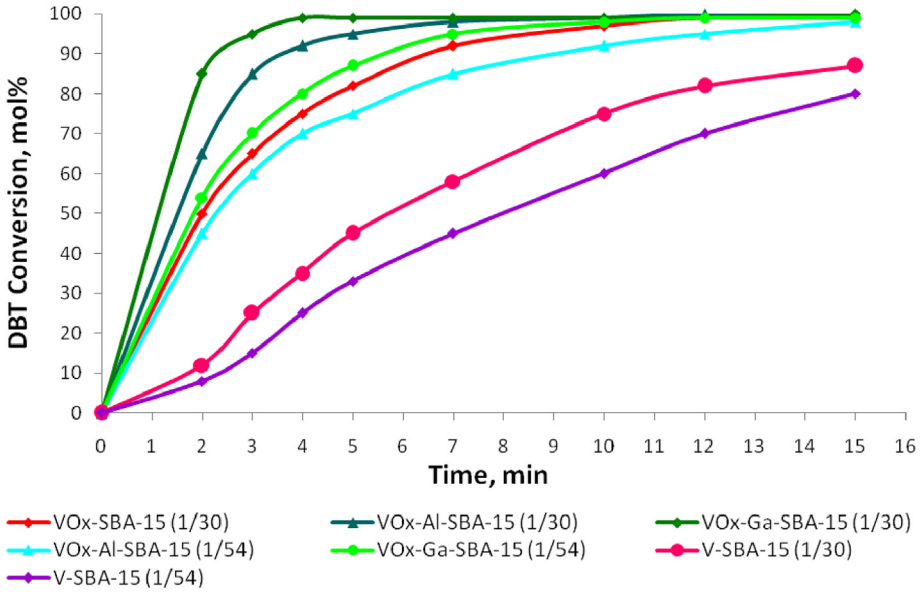

Fig. 19. Catalytic activity of the samples modified with heteroatom (V, Al and Ga) with different V/Si ratios. Molar ratio O/S = 12, T = 60 °C. g DBT/g cat = 0.96 (500 ppm). Note: VOx-SBA-15 (1/30) is shown again for comparison.

D. Huang et al. [98] reported that in DBT oxidation to the corresponding DBT sulfones. The sulfones, which are more polar than DBT, adsorb onto the surface of the catalyst, leading to fewer active sites which have access to the reactant during oxidation. In addition Jia et al. [99] assumed that the competition of adsorption between DBT and the sulfones on the catalyst under relative high sulfur concentration resulted in the decrease of the DBT oxidation rate.

On the other hand, various Bronsted acidic ILs have also been reported to be the ODS catalysts [100–102], where acidic ILs offer a high reaction rate to the conversion of S-compounds. Several papers demonstrated the co-catalysis effect of Bronsted acidic groups for the oxidative reaction of S-compounds [103,104]. The hydrogen bonds formed between active H and S atoms enhance the oxidative reactivities of S-compounds and further promote the sulfur removal efficiency. In this way, the Bronsted-Lewis acidic ILs may lead to a qualitative leap in desulfurization efficiency.

Kumar et al. [105] found that the introduction of Bronsted acid sites in the H + -exchanged manganese oxide molecular sieves plays an important role in cyclohexane oxidation and contributes in achieving higher conversion and higher selectivity for the desired product. The proposed mechanism supports the dual active site participation in the oxidation process.

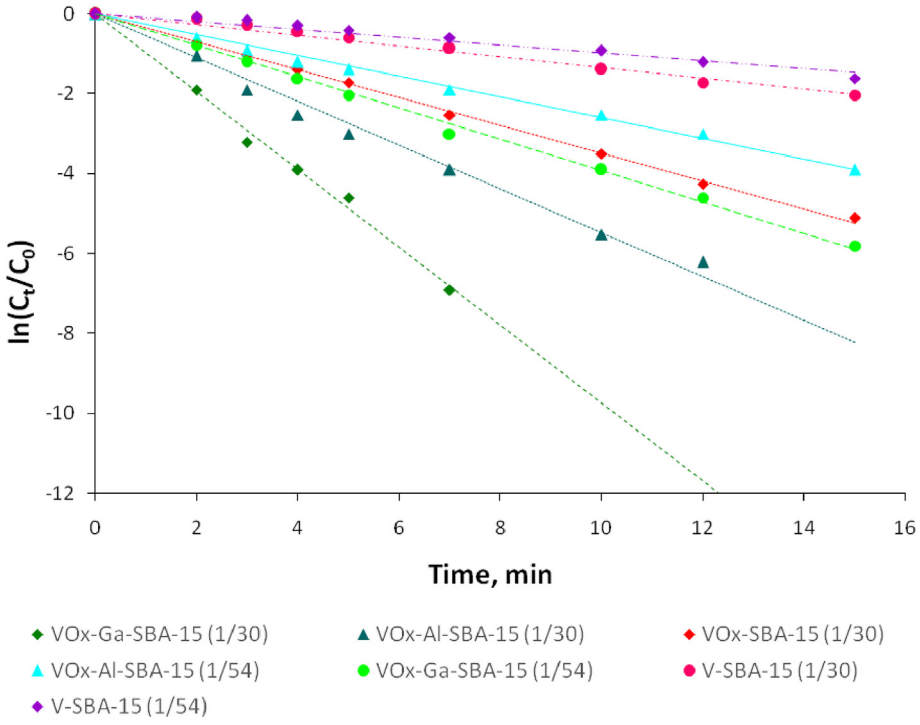

Fig. 20. Pseudo first-order kinetic. Molar ratio O/S = 12, T = 60 °C. g DBT/g cat = 0.96 (500 ppm).

Table 4
Apparent kinetic rate constant obtained applying pseudo first-order kinetic: $\ln(C_t/C_0) = -kt$.

Samples	Apparent kinetic rate constant (min^{-1})	T(°C)	R^2
V-SBA-15 (1/30)	0.097	60	0.98
V-SBA-15 (1/54)	0.134	60	0.96
VOx-SBA-15 (1/30)	0.348	60	0.98
VOx-Al-SBA-15 (1/54)	0.260	60	0.99
VOx-Al-SBA-15 (1/30)	0.547	60	0.98
VOx-Ga-SBA-15 (1/54)	0.390	60	0.97
VOx-Ga-SBA-15 (1/30)	0.975	60	0.99
VOx-Ga-SBA-15 (1/30)	0.458	50	0.99
VOx-Ga-SBA-15 (1/30)	0.645	40	0.99

To make a more detailed comparison, the reaction rate constant over the most active catalysts was calculated. The ODS of dibenzothiophene follows a pseudo first-order kinetics, according to previous results, obtained on solid catalysts [23,106–109]. Thus, Equations (1) And (2) were used to obtain the kinetic parameters. The fittings are shown in Fig. 20 and the values obtained are listed in Table 4.

Obviously, VOx-Ga-SBA-15 displayed the highest reaction rate constant, reaching 0.975 min^{-1} at 60 °C, which is 1.8 times higher in VOx-Al-SBA-15 and 3 times higher in VOx-SBA-15 with the same V/Si ratio of 1/30. Such catalytic reactivity is much better than 0.067 min^{-1} obtained in our previous work using anatase supported-

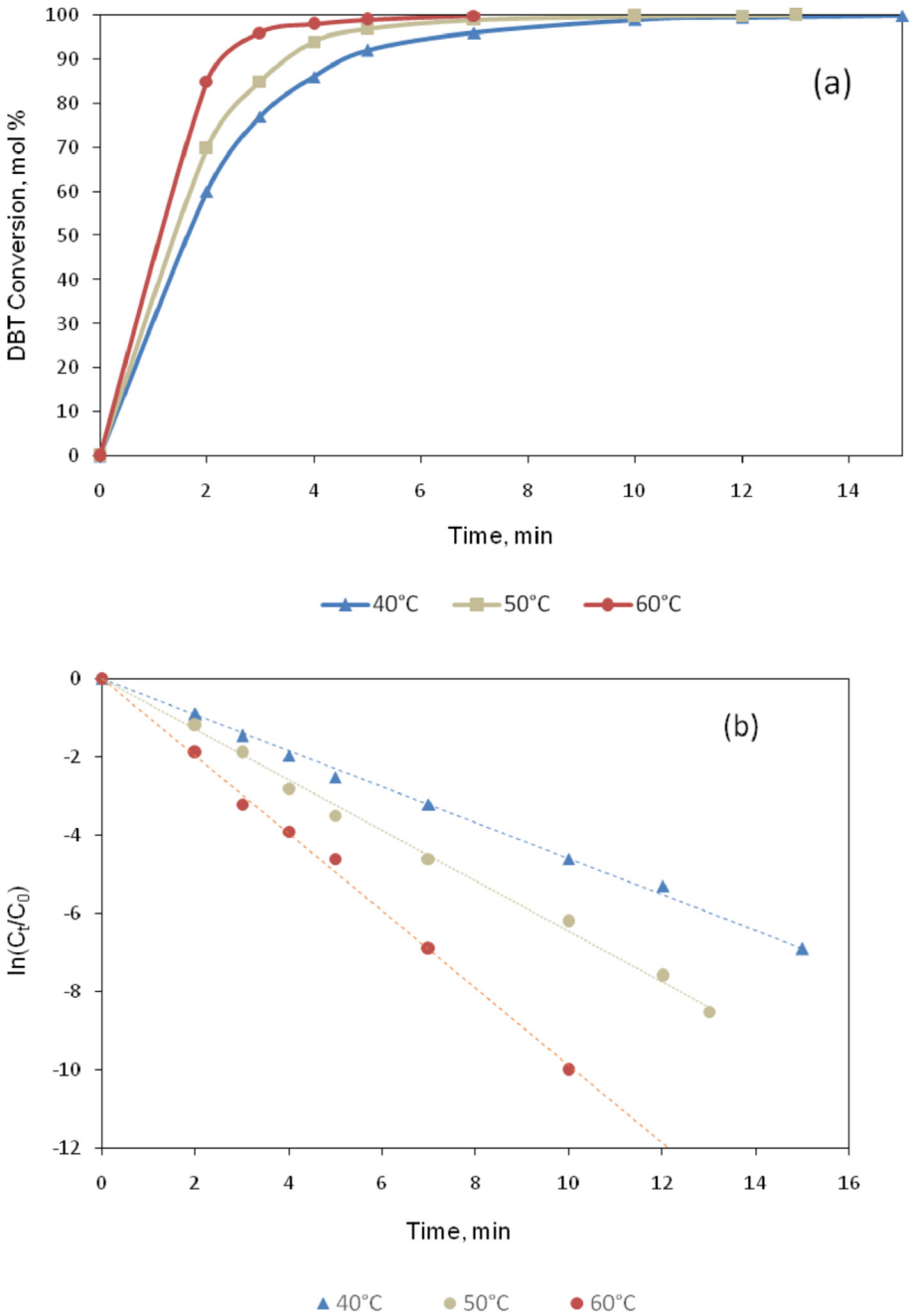

Fig. 21. (a) Catalytic activity of VOx-Ga-SBA-15 (1/30) under different reaction temperatures. (b) First order fitting of VOx-Ga-SBA-15 (1/30) under different reaction temperatures. Molar ratio O/S = 12, g DBT/g cat = 0.96 (500 ppm).

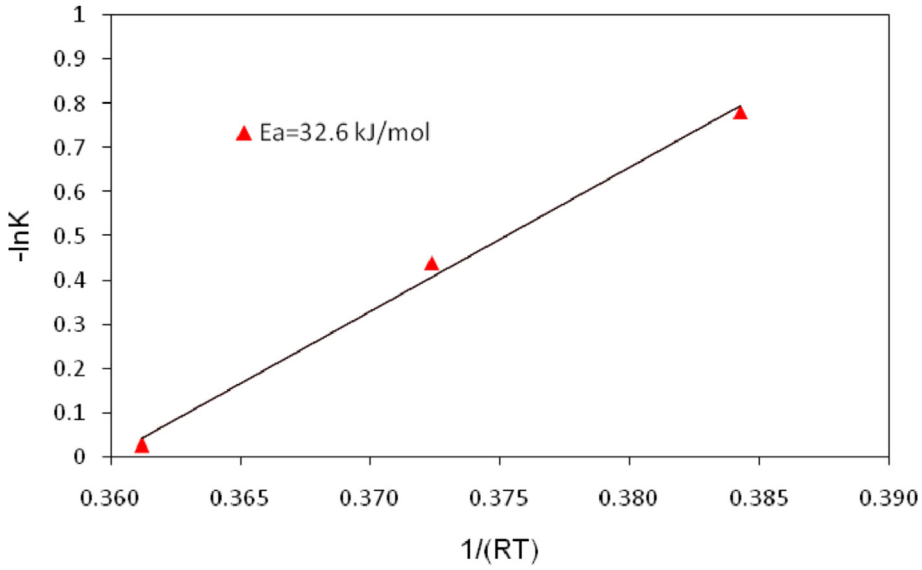

Fig. 22. Arrhenius plot for VOx-Ga-SBA-15 (1/30).

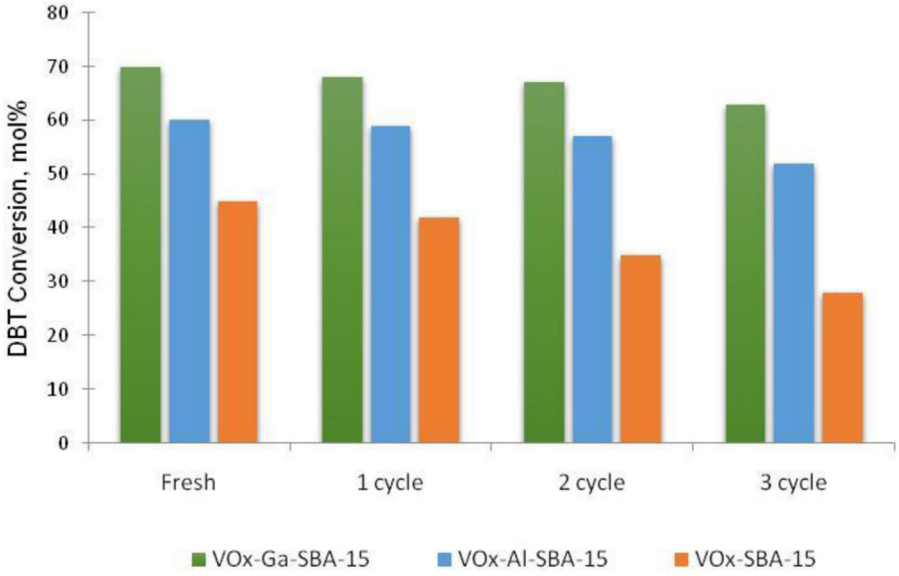

Fig. 23. Deactivation study of vanadium samples (V/Si = 30) at 10 min of reaction time. Molar ratio H_2O_2/DBT = 6 (O/S = 12), T = 60 °C, g DBT/g cat = 1.92, in L–S phase system.

SBA-16 [23] and 4 times faster than using V-CMK-3, with higher vanadium content at the same temperature [24].

The effect of temperature was evaluated over the most active VOx-Ga-SBA-15 (1/30) catalyst. The ODS of DBT was tested by varying temperature from 40, 50 and 60 °C without altering the other conditions. The catalytic activity and the pseudo first-order fitting are displayed in Fig. 21 (a) and (b), respectively. The Arrhenius plot is shown in Fig. 22. The calculated Ea value for the oxidation of DBT was 32.6 kJ/mol. This value is lower compared with that of our previous work using anatase supported-SBA-16, where Ea was 43.4 kJ/mol [23]. Ea for DBT ODS published in other works was 52.83 kJ/mol using polyoxometalates as catalysts and hydrogen peroxide/acetic as oxidant [110], 60 kJ/mo1 in H_2O_2/formic acid [111], and 56 kJ/mol in a similar system using crystalline forms of nano-TiO_2 [108]. Bazyari et al. [107] obtained 0.199 min^{-1} using microporous titania-silica at 80 °C. Studies on vanadium catalysts applied to the ODS of DBT were reported in the literature. Alvarez-Amparán et al. [112] studied the performance of MoOx-VOx-based catalysts in the ODS process, using Al_2O_3 as catalytic support, and hydrogen peroxide as oxidants agents. The MoOx-VOx interaction promoted VOx distribution, mainly as isolated-vanadium species. The best catalyst with 5 wt % Mo and 15 wt % V reached 97% of conversion. The rate constant was 0.052 min^{-1} at 60 °C. Cedeño Caero et al. [19] performed the ODS of DBT over TiO_2 anatase-supported V_2O_5 (10 wt%). The rate constant obtained at 70 °C was 0.41 min^{-1} and the apparent activation energy was 35.3 kJ/mol.

3.3. Deactivation of the catalyst

Regenerability is an important parameter for catalytic materials to be considered for practical applications. The catalysts used were regenerated by oxidative air treatment and the experimental conditions were the same as those described above. However, in this

study, the amount of catalysts was lowered to 30 mg to avoid working at high conversion levels close to 100%. In Fig. 23 we observe that the activity of the sample used remains after the third recycle compared to a fresh catalyst. This indicates that no vanadium leaching occurs during the reaction. The reusability of the catalysts indicate that VOx-SBA-15 and VOx-SBA-15 modified with Ga and Al are potential catalysts for the ODS of dibenzothiophene.

4. Conclusions

It was observed that the sulfone yield is not proportional to the vanadium content but that the characteristics of the support are the most important aspects. We conducted ODS of DBT in the presence of vanadium oxides in several supports. Incorporation of aluminum and gallium in tetrahedral positions improves dispersion of vanadium species, probably due to a better anchorage of the active species on a more acidic support. The use of Ga-SBA-15 support applied to the ODS of sulfur compounds was not found in the literature. The results show the total S-removal using Ga-SBA-15 support with 2-3 wt% of vanadium mainly as V^{+5} isolated species. The reusability of the catalysts indicates that VOx-SBA-15 modified with Ga and Al are potential catalysts for the ODS of dibenzothiophene.

Acknowledgment

Lorena Rivoira, María L. Martínez, Oscar Anunziata and Andrea Beltramone. NANOTEC, , National Technology University, Cordoba Faculty, Maestro Lopez y Cruz Roja Argentine. We acknowledge the financial support of CONICET Argentina, PIP CONICET 11220120100218CO. 2014–2017. We thank Dr. J. L. Garcia Fierro for XPS analysis.

Appendix A. Supplementary data

Supplementary data related to this article can be found at http://dx.doi.org/10.1016/j.micromeso.2017.04.019.

References

[1] M.T. Timko, J.A. Wang, J. Burgess, P. Kracke, L. Gonzalez, C. Jaye, D.A. Fischer, Fuel 163 (2016) 223–231.
[2] K.S. Triantafyllidis, E.A. Deliyanni, Chem. Eng. J. 236 (2014) 406.
[3] H. Gomez-Bernal, L. Cedeño-Caero, A. Gutierrez-Alejandre, Catal. Today 142 (2009) 227.
[4] J. Xiao, L. Wu, Y. Wu, B. Liu, L. Dai, Z. Li, Q. Xia, H. Xi, Appl. Energy 113 (2014) 78.
[5] O. Gonzalez-Garcia, L. Cedeño-Caero, Catal. Today 150 (2010) 237.
[6] X. Chen, D. Song, C. Asumana, G. Yu, J. Mol. Catal. A Chem. 359 (2012) 8.
[7] W.A. Bakar, R. Ali, A.A. Kadir, W.N. Mokhtar, Fuel Process. Technol. 101 (2012) 78.
[8] H. Shang, H. Zhang, W. Du, Z. Liu, Ind. Eng. Chem. 19 (2013) 1426.
[9] E. Rafiee, S. Eavani, J. Ind. Eng. Chem. 380 (2013) 18.
[10] Z. Eldin, A. Abdalla, B. Li, Chem. Eng. J. 113 (2012) 200.
[11] L. Cedeño-Caero, M. Ramos-Luna, M. Mendez-Cruz, J. Ramirez-Solis, Catal. Today 172 (2011) 189–194.
[12] I.V. Babich, J.A. Moulijn, Fuel 82 (2003) 607.
[13] E. Ito, J.A.R. van Veen, Catal. Today 116 (2006) 446.
[14] E.W. Qian, J. Jpn. Petrol. Inst. 51 (2008) 14.
[15] D. Wang, E.W. Qian, H. Amano, K. Okata, A. Ishihara, T. Kabe, Appl. Catal. A Gen. 253 (2003) 91.
[16] L. Cedeño-Caero, H. Gomez-Bernal, A. Fraustro-Cuevas, H.D. Guerra-Gomez, R. Cuevas-Garcia, Catal. Today 133–135 (2008) 244.
[17] E. Torres-Garcia, G. Canizal, S. Velumani, L. Ramirez-Verduzco, F. Murrieta-Guevara, J. Ascencio, Appl. Phys.A-Mater. Sci. Process 79 (2004) 2037.
[18] B. Zapata, F. Pedraza, M.A. Valenzuela, Catal. Today 106 (2007) 219.
[19] L. Cedeño Caero, E. Hernández, F. Pedraza, F. Murrieta, Catal. Today 564 (2005) 107–108.
[20] Y. Shiraishi, T. Naito, T. Hirai, Ind. Eng. Chem. Res. 42 (2003) 6034.
[21] A.V. Anisimov, E.V. Fedorova, A.Z. Lesnugin, V.M. Senyavin, L.A. Aslanov, V.B. Rybakov, A.V. Tarakanova, Catal. Today 78 (2003) 319.
[22] Y.-M. Liu, Y. Cao, N. Yi, W.-L. Feng, W.-L. Dai, S.-R. Yan, H.-Y. He, K.-N. Fan, J. Catal. 224 (2004) 417–428.
[23] L.P. Rivoira, V.A. Vallés, B.C. Ledesma, M.V. Ponte, M.L. Martínez, O.A. Anunziata, A.R. Beltramone, Catal. Today 271 (2016) 102–113.
[24] L.P. Rivoira, J.M. Juárez, H. Falcón, M. Gómez Costa, O.A. Anunziata, A.R. Beltramone, Catal. Today 282 (part 2) (2017) 123132.
[25] G. Du, S. Lim, M. Pinault, C. Wang, F. Fang, L. Pfefferle, G.L. Haller, J. Catal. 253 (2008) 74–90.
[26] A. Khodakov, J. Yang, S. Su, E. Iglesia, A.T. Bell, J. Catal. 177 (1998) 343.
[27] A. Khodakov, B. Olthof, A.T. Bell, E. Iglesia, J. Catal. 181 (1999) 205.
[28] M. Puglisi, F. Arena, F. Frusteri, V. Sokolovskii, A. Parmaliana, Catal. Lett. 41 (1996) 41.
[29] D. Srinivas, P. Ratnasamy, Microporous Mesoporous Mater. 105 (2007) 170.
[30] W. Ding, W. Zhu, J. Xiong, L. Yang, A. Wei, M. Zhang, H. Li, Chem. Eng. J. 266 (2015) 213.
[31] K.-S. Cho, Y.-K. Lee, App. Catal. B Env. 147 (2014) 35.
[32] Y. Wei, Y. Li, Y. Tan, Z. Wua, L. Pan, Y. Liu, Chem. Eng. J. 298 (2016) 271–280.
[33] X. Zhang, H. Dong, Y. Wang, N. Liu, Y. Zuo, L. Cui, Chem. Eng. J. 283 (2016) 1097–1107.
[34] M.J. Gracia, E. Losada, R. Luque, J.M. Campelo, D. Luna, J.M. Marinas, A.A. Romero, Appl. Catal. A 349 (2008) 148–155.
[35] D. Zhao, J. Feng, Q. Huo, N. Melosh, G. Fredrickson, B. Chmelka, G. Stucky, Science 279 (1998) 548.
[36] M.J. Remy, M.J. Genet, G. Poncelet, P.F. Lardinois, P.P. Notte, J. Phys. Chem. 96 (1992) 2614.
[37] J. Goscianska, A. Olejnik, I. Nowak, M. Marciniak, R. Pietrzak, Eur. J. Pharm. Biopharm. 94 (2015) 550.
[38] S. Chytil, L. Haugland, E.A. Blekkan, Microporous Mesoporous Mater. 111 (2008) 134.
[39] A. Tadjarodia, F. Zabihia, S. Afshara, Ceram. Int. 39 (2013) 7649.
[40] I.M. El-Nahhal, J.K. Salem, M. Selmane, F.S. Kodeh, H.A. Ebtihan, Chem. Phys. Lett. 667 (2017) 165.
[41] I. Mazilu, C. Ciotonea, A. Chirieac, B. Dragoi, C. Catrinescu, A. Ungureanu, S. Petit, Se Royer, E. Dumitriu, Microporous Mesoporous Mater. 241 (2017) 326.
[42] R. Barthos, A. Hegyessy, S. Klébert, J. Valyon, Microporous Mesoporous Mater. 207 (2015) 1–8.
[43] J. Klinowski, Ann. Rev. Mater. Sci. 18 (1988) 189–218.
[44] B. Jarry, F. Launay, J.P. Nogier, V. Montouillout, L. Gengembre, J.L. Bonardet, Appl. Catal. A Gen. 309 (2006) 177–186.
[45] C.K.H. Timken, E. Oldfield, J. Am. Chem. Soc. 109 (1987) 7669–7673.
[46] K. Okumura, K. Nishigaki, M. Niwa, Microporous Mesoporous Mater. 44–45 (2001) 509–516.
[47] B. Solsona, T. Blasco, J.M.L. Nieto, M.L. Peña, F. Rey, A. Vidal-Moya, J. Catal. 203 (2001) 443.
[48] H. Eckert, I.E. Wachs, J. Phys. Chem. 93 (1989) 6796.
[49] O.B. Lapina, V.M. Mastikhin, A.A. Shubin, V.N. Krasilnikov, K.I. Zamarev, Prog. Nucl. Magn. Reson. Spectrosc. 24 (1992) 457.
[50] H. Berndt, A. Martin, A. Bruckner, E. Schreier, D. Muller, H. Kosslick, G.V. Wolf, B. Lucke, J. Catal. 191 (2000) 284.
[51] D. Wei, H. Wang, X. Feng, W.-T. Chueh, P. Ravikovitch, M. Lyubovsky, C. Li, T. Takeguchi, G.L. Haller, J. Phys. Chem. B 103 (1999) 2113.
[52] F. Gao, Y. Zhang, H. Wan, Y. Kong, X. Wu, L. Dong, B. Li, Y. Chen, Micropor. Mesopor. Mater. 110 (2008) 508–516.
[53] C. Lin, K. Tao, H.B. Yu, D.Y. Hua, S.H. Zhou, Catal. Sci. Technol. 4 (2014) 4010–4019.
[54] D.E. Keller, T. Visser, F. Soulimani, D.C. Koningsberger, B.M. Weckhuysen, Vib. Spectrosc. 43 (2007) 140–151.
[55] M. Mathieu, P. Van Der Voort, B.M. Weckhuysen, R.R. Rao, G. Catana, R.A. Schoonheydt, E.F. Vansant, J. Phys. Chem. B 105 (2001) 3393–3399.
[56] M. Piumetti, B. Bonelli, M. Armandi, L. Gaberova, S. Casale, P. Massiani, E. Garrone, Micropor. Mesopor. Mater. 133 (2010) 36–44.
[57] Y.M. Liu, Y. Cao, N. Yi, W.L. Feng, W.L. Dai, S.R. Yan, J. Catal. 224 (2004) 417–428.
[58] M. Baltes, K. Cassiers, P. Van der Voort, B.M. Weckhuysen, R.A. Schoonheydt, E.F. Vansant, J. Catal. 197 (2001) 160–171.
[59] M.A. Larrubia, G. Busca, Mater. Chem. Phys. 72 (2001) 337–346.
[60] J.G. Eon, R. Olier, J.C. Volta, J. Catal. 145 (1994) 318–326.
[61] P. Concepción, M.T. Navarro, T. Blasco, J.M. López Nieto, B. Panzacchi, F. Rey, Catal. Today 96 (2004) 179–186.
[62] G. Catana, R. Ramachandra Rao, B.M. Weckhuysen, P. Van Der Voort, E. Vansant, R.A. Schoonheydt, J. Phys. Chem. B 102 (1998) 8005–8012.
[63] J.C. Dupin, D. Gonbeau, P. Vinatier, A. Levasseur, Phys. Chem. Chem. Phys. 2 (2000) 1319–1324.
[64] J. Fang, X. Bi, D. Si, Z. Jiang, W. Huang, Appl. Surf. Sci. 253 (2007) 8952–8961.
[65] M.D. Soriano, J.A. Cecilia, A. Natoli, J. Jiménez, J.M. López Nieto, E. Rodríguez-Castellón, Catal. Today 254 (2015) 36–42.
[66] S. Dzwigaj, P. Massiani, A. Davidson, M. Che, J. Mol. Catal. A Chem. 155 (2000) 169–182.
[67] L. Capek, R. Bulanek, J. Adam, L. Smolakova, H. Sheng-Yang, P. Cicmanec, Catal. Today 141 (2009) 282–287.
[68] M. Demeter, M. Neumann, W. Reicheit, Surf. Sci. 454 (2000) 41.
[69] M. Fraldos, J.A. Anderson, M.A. Banares, J.L.G. Fierro, S.W. Weller, J. Catal. 168 (1997) 110 (and references therein).
[70] J. George, S. Shylesh, A.P. Singh, Appl. Catal. A General 290 (2005) 148–158.

[71] G. Silversmit, D. Depla, H. Poelman, G.B. Marin, R. De Gryse, J. Electron Spectrosc. Relat. Phenom. 135 (2004) 167–175.
[72] S. Yoshida, T. Tanaka, T. Hanada, T. Hiraiwa, H. Kanai, T. Funabiki, Catal. Lett. 12 (Issue 1) (1992) 277–285.
[73] A. Abidli, S. Hamoudi, K. Belkacemi, Dalton Trans. 44 (2015) 9823–9838.
[74] A. Pashutski, A. Hoffman, M. Folman, Surf. Sci. 208 (1898) L91.
[75] M. Gomez-Cazalilla, J.M. Merida-Robles, A. Gurbani, E. Rodriguez-Castellon, A. Jimenez-Lopez, J. Solid State Chem. 180 (2007) 1130–1140.
[76] J.M. Merida-Robles, P. Olivera Pastor, A. Jimenez Lopez, E. Rodrıguez Castellon, J. Phys. Chem. 100 (1996) 14726.
[77] S. Chen, Z. Qin, X. Xu, J. Wang, Appl. Catal. A-Gen. 302 (2006) 185–192.
[78] F. Arena, F. Frusteri, A. Parmaliana, Appl. Catal. A-Gen. 176 (1999) 189–199.
[79] J. Santamaría-González, J. Luque-Zambrana, J. Mérida-Robles, P. Maireles-Torres, E. Rodríguez-Castellón, A. Jiménez-López, Catal. Lett. 68 (2000) 67–73.
[80] M.S. Park, V.P. Vislovskiy, J.S. Chang, Y.G. Shul, J.S. Yoo, S.E. Park, Catal. Today 87 (2003) 205–212.
[81] H. Dai, A.T. Bell, E. Iglesia, J. Catal. 221 (2004) 491–499.
[82] B. Solsona, J.M.L. Nieto, U. Díaz, Micropor. Mesopor. Mater. 94 (2006) 339–347.
[83] M.C. Carrión, B.R. Manzano, F.A. Jalón, I. Fuentes-Perujo, P. Maireles-Torres, E. Rodríguez-Castellón, A. Jiménez-López, Appl. Catal. A 288 (2005) 34–42.
[84] D.J. Ostgard, L. Kustov, K.R. Poeppelmeier, W.M.H. Sachtler, J. Catal. 133 (1992) 342–357.
[85] R. Bulánek, P. Cicmanec, H. Sheng-Yang, P. Knotek, L. Capek, M. Setnicka, Appl. Catal. A Gen. 415–416 (2012) 29–39.
[86] C.A. Carrero, R. Schloegl, I.E. Wachs, R. Schomaecker, ACS Catal. 4 (2014) 3357–3380.
[87] Y.-M. Liu, W.-L. Feng, T.-C. Li, H.-Y. He, W.-L. Dai, W. Huang, Y. Cao, K.-N. Fan, J. Catal. 239 (2006) 125–136.
[88] G. Mitran, T. Cacciaguerra, S. Loridant, D. Tichit, I.-C. Marcu, Appl. Catal. A Gen. 417–418 (2012) 153–162.
[89] A. Galarneau, M. Nader, F. Guenneau, F. Di Renzo, A. Gedeon, J. Phys. Chem. C 111 (2007) 8268–8277.
[90] G. Xiong, C. Li, H.Y. Li, Q. Xin, Z.C. Feng, Chem. Commun. (2000) 677–678.
[91] C. Li, J. Catal. 216 (2003) 203–212.
[92] M.V. Bosco, M.A. Bañares, M.V. Martínez-Huerta, A.L. Bonivardi, S.E. Collins, J. Mol. Catal. A Chem. 408 (2015) 75–84.
[93] A. Gonzalo, E. Nogales, B. Méndez, J. Piqueras, Phys. Stat. Sol. A 211 (2014) 494–497.
[94] D. Dohy, G. Lucazeau, A. Revcolevschi, J. Sol. State Chem. 45 (1982) 180–192.
[95] T.A. Zepeda, A. Infantes-Molina, J.N. Díaz de Leona, R. Obeso-Estrella, S. Fuentes, G. Alonso-Nuñeza, B. Pawelec, J. Mol. Catal. 397 (2015) 26–35.
[96] T. Barzetti, E. Selli, D. Moscotti, L. Forni, J. Chem. Soc. Faraday Trans. 92 (1996) 1401–1407.
[97] T.R. Hughes, H.M. White, J. Phys. Chem. 71 (1967) 2192–2201.
[98] D. Huang, Y.J. Wang, Y.C. Cui, G.S. Luo, Microporous Mesoporous Mater. 116 (2008) 378–385.
[99] Y. Jia, G. Li, G. Ning, Fuel Process. Technol. 92 (2011) 106–111.
[100] H. Gao, C. Guo, J. Xing, J. Zhao, H. Liu, Green Chem. 12 (2010) 1220–1224.
[101] J. Gui, D. Liu, Z. Sun, D. Liu, D. Min, B. Song, X. Peng, J. Mol. Catal. A-Chem. 331 (2010) 64–70.
[102] W. Zhang, K. Xu, Q. Zhang, D. Liu, S. Wu, F. Verpoort, X.-M. Song, Ind. Eng. Chem. Res. 49 (2010) 11760–11763.
[103] B. Zhang, Z. Jiang, J. Li, Y. Zhang, F. Lin, Y. Liu, C. Li, J. Catal. 287 (2012) 5–12.
[104] H. Lu, S. Wang, C. Deng, W. Ren, B. Guo, J. Hazard. Mater. 279 (2014) 220–225.
[105] R. Kumar, S. Sithambaram, S.L. Suib, J. Catal. 262 (2009) 304–313.
[106] N.D. McNamara, J.C. Hicks, ACS Appl. Mater. Interfaces 7 (2015) 5338–5346.
[107] A. Bazyari, A.A. Khodadadi, A. Haghighat Mamaghani, J. Beheshtian, L.T. Thompson, Y. Mortazavi, Appl. Catal. B 180 (2016) 65–77.
[108] L. Li, J. Zhang, C. Shen, Y. Wang, G. Luo, Fuel 167 (2016) 9–16.
[109] Z. Hasan, J. Jeon, S.H. Jhung, J. Hazard. Mater 205–206 (2012) 216–221.
[110] C. Komintarachat, W. Trakarnpruk, Ind. Eng. Chem. Res. 45 (2006) 1853.
[111] H. Ling, B.X. Shen, X.L. Zhou, Z.J. Gang, J. East China Univ. Sci. Technol. Nat. Sci. Ed.) 31 (2005) 48.
[112] M.A. Alvarez-Amparán, L. Cedeño-Caero, Catal. Today 282 (part 2) (2016) 133–139.